The Astrophysical Journal, 843:132 (18pp), 2017 July 10 https://doi.org/10.3847/1538-4357/aa7513

Characteristics of Solar Energetic Ions as a Function of Longitude

C. M. S. Cohen[1], G. M. Mason[2], and R. A. Mewaldt[1]
[1] California Institute of Technology, MC 290-17, Pasadena, CA 91125, USA; cohen@srl.caltech.edu
[2] Johns Hopkins University/Applied Physics Laboratory, Laurel, MD 20723, USA
Received 2017 March 23; revised 2017 May 22; accepted 2017 May 23; published 2017 July 13

Abstract

Since the 2006 launch of *STEREO*, multi-spacecraft studies have yielded several surprising results regarding the spread of solar energetic particles (SEPs) within the inner heliosphere. We have investigated the role of energy and ridigity, using *ACE* and *STEREO* 10 MeV n^{-1} oxygen data to identify 41 large SEP events observed by two or three spacecraft. We calculated fluence spectra from ~0.1 to >10 MeV n^{-1} for H, He, O, and Fe for each event at the observing spacecraft (including *SOHO* and *GOES*). The particle fluences at 0.3, 1, and 10 MeV n^{-1} were examined as a function of the distance between the associated solar flare longitude and the spacecraft magnetic footpoints at the Sun to determine the longitudinal spread of particles and study how the distribution centers and widths depend on energy and charge-to-mass (Q/M) for the first time. On average, the three-spacecraft event distributions were centered at 22 ± 4° west of the flare site and were 43 ± 1° wide, though there was substantial variability, while the fit to the aggregate of the two-spacecraft event fluences yielded significantly wider distributions at 0.3 and 1 MeV n^{-1}. The widths derived from both the three- and two-spacecraft events show an energy dependence with distributions narrowing with increasing energy, consistent with lower energy ions experiencing more field line co-rotation, or being accelerated over a larger portion of the CME-driven shock or for longer times as the shock expands. Surprisingly, no clear evidence was found for a Q/M dependence to the widths or centers suggesting that rigidity-related processes are not the dominant means of spreading particles in longitude.

Key words: acceleration of particles – interplanetary medium – solar–terrestrial relations – Sun: coronal mass ejections, (CMEs) – Sun: flares – Sun: particle emission

1. Introduction

The processes that result in solar energetic particle (SEP) events observed near 1 au can be placed into two broad categories: those related to the acceleration of the particles and those related to their transport between the Sun and 1 au. Unfortunately, from single spacecraft measurements at a single location, it is nearly impossible to disentangle the effects of acceleration versus transport processes. Information regarding the solar source of SEPs is typically limited to remote sensing observations of active regions, flares, and coronal mass ejections (CMEs) with almost no information on the conditions of the interplanetary medium between a few tenths of an au and 1 au. However, these conditions significantly affect the acceleration and transport processes, which determine the abundances, fluences, and composition of the resulting SEP events and how these characteristics vary in time and space.

The longitudinal spread of SEPs has been studied for decades, often inferred from single spacecraft measurements near Earth combined with the observed location of the associated active region or flare on the Sun (e.g., Cane et al. 1986; Reames 1999; Van Hollebeke et al. 1975). For large SEP events associated with CMEs, the detection of particles at a spacecraft, whose magnetic footpoint at the Sun (as determined by a standard Parker spiral; Nolte & Roelof 1973) is well removed from the associated solar active region, is typically explained by the large longitudinal extent of the CME-driven shock responsible for accelerating the SEPs (Mason et al. 1984; Cane et al. 1988). However, the longitudinal extent of the accelerating shock is typically assumed to be <180° (Cane 1988), roughly centered over the associated active region, and several examples exist of SEP events detected where the longitudinal spread between the spacecraft solar footpoint and the solar source region was >120° (e.g., Cliver et al. 1995, 2005). These anomalously wide events have led to debates regarding the presence of circumsolar coronal shocks (Cliver et al. 1995) and cross-field diffusion in the interplanetary medium (Zhang et al. 2003, and references therein).

Prior to 2006, the opportunities for using multiple spacecraft to measure the longitudinal spread of SEPs were limited with the two-spacecraft *Helios* mission yielding the best determination of the typical longitudinal extent of SEP events. However, the *Helios* spacecraft were typically separated from each other and near-Earth satellites in both longitude and radius, making it difficult to disentangle longitudinal from radial variations in SEP event characteristics (Lario et al. 2006; Reames et al. 2013). The SEP sensors on *Helios* were also limited to electron, proton, and alpha measurements, making it impossible to study aspects such as the variation in SEP heavy ion composition and related charge-to-mass (Q/M) dependences in the longitudinal spread.

The *STEREO* mission was designed to examine the characteristics of SEPs from multiple vantage points. The sensors on the twin *STEREO* spacecraft are similar to those on near-Earth spacecraft such as *ACE*, measuring H-Fe intensities over more than 2 orders of magnitude in energy. By combining data from *STEREO* and *ACE*, variations in composition and spectra can be studied as a function of longitude without the complications of radial-dependent effects. The *STEREOs* also carry imaging instruments, which allow multiple views of the solar surface and coronagraph images of CMEs. Between 2011 February and 2014 October, the separation of the two *STEREO* spacecraft was large enough that, in combination with near-Earth imaging capabilities, the entire surface of the Sun could be continually monitored, allowing observations of the solar source of an SEP event regardless of its location on the Sun.

Several surprising results have been obtained from SEP studies using *STEREO* and near-Earth spacecraft. Richardson et al. (2014) found that SEP events with solar sources on the solar hemisphere not in view of the observing spacecraft (referred to here as the "backside" of the Sun) are not uncommon and amount to ~30% of SEP events detected in >25 MeV protons (see also Shea & Smart 1990). The 2011 November 3 event resulted in onsets of >25 MeV protons at spacecraft nearly evenly distributed around the Sun within 30 minutes of each other (Mewaldt et al. 2013; Richardson et al. 2014). Observations of energetic electron events and measurements of their anisotropies at multiple spacecraft have also shown surprisingly efficient and wide longitudinal distribution (Dresing et al. 2014). It was understood that smaller SEP events, enriched in ^{3}He, were only observable when the spacecraft was within a cone of approximately ±20° centered on the magnetic connection to the compact solar source (Reames 1999). However, multi-spacecraft measurements of these events have shown that not infrequently they can extend over ⩾60° and as wide as 136° (Wiedenbeck et al. 2011, 2013).

These results point toward efficient and rapid distribution of particles throughout the inner heliosphere, at least under certain conditions. Whether this is a result of transport alone, a broad source region close to the Sun or a combination of both is unclear. Without in situ measurements near the Sun where much of the particle acceleration is occurring (especially at high energies; Mewaldt et al. 2003), we must rely on theory and modeling to deduce the transport and acceleration conditions. Longitudinal SEP studies made at ~1 au are useful for constraining and testing such models.

In this study, we use *ACE* and *STEREO* data to survey 41 large SEP events, which were detected in 10 MeV n^{-1} oxygen by two or more spacecraft (the requirement of high energy measurements simplified the identification of the solar source). By statistically studying the longitudinal characteristics of heavy ions at several energies, organization with Q/M ratios and energy can be examined. We have also included analysis of *SOHO* and *GOES* SEP intensities to compare the characteristics of heavy ions to those of protons. Lario et al. (2013) and Richardson et al. (2014) previously used *STEREO* to examine the longitudinal distribution of proton peak intensities in SEP events, and Lario et al. (2006) used *Helios* data to study energetic protons and electrons; however, there has not been a study that focused on heavy ions to address the role of Q/M-related processes or examined so broad an energy range.

The composition results of this survey will also have bearing on the theories that have been put forth to explain large SEP events with uncommonly high Fe/O ratios (Cohen et al. 1999; Mason et al. 1999). Two of the prevailing theories suggest different longitudinal dependences to the Fe/O ratio: the direct-flare contribution scenario posits that the high Fe/O ratios are signatures of SEPs accelerated by flare-related processes and are being observed by an observer well connected to the flare site (Cane et al. 2003), while the seed population explanation suggests that the enhanced abundances are a reflection of the local seed population accelerated by the CME-driven shock (Tylka et al. 2005). A longitudinal dependence to the Fe/O ratio, with higher Fe/O values at the center of the particle distribution, would support the direct-flare contribution idea, while no longitude dependence would favor the seed population idea (for further discussion, see Cohen et al. 2013).

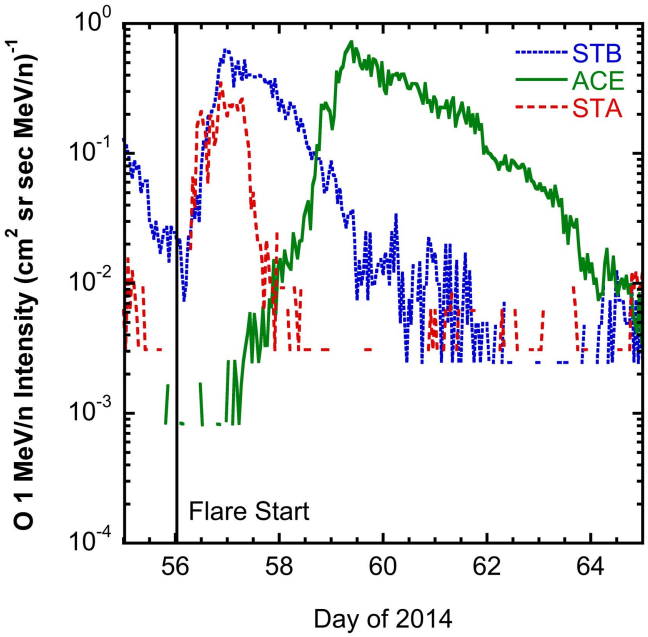

Figure 1. Hourly oxygen intensities at 1 MeV n^{-1} as measured by *STB*, *ACE*, and *STA* for the 2014/056 three-spacecraft event. The start time of the associated flare is indicated by the black vertical line.

2. Observations

2.1. Instrument and Event Selection

For the heavy ion measurements, we analyzed data from the Suprathermal Ion Telescope (SIT; Mason et al. 2008) and the Low Energy Telescope (LET; Mewaldt et al. 2008) on the two *STEREO* spacecraft and the Ultra-Low Energy Isotope Spectrometer (ULEIS; Mason et al. 1998) and the Solar Isotope Spectrometer (SIS; Stone et al. 1998a) on *ACE*. We obtained proton data from the Solar Electron Proton Telescope (SEPT; Müller-Mellin et al. 2008) and LET on *STEREO*; the Electron, Proton, Alpha Monitor (EPAM; Gold et al. 1998), and ULEIS on *ACE*; the Electron Proton Helium Instrument (EPHIN; Müller-Mellin et al. 1995) on *SOHO*; and the Energetic Particle Sensor (EPS) on the *GOES* satellite. The heavy ion measurements on *STEREO* and *ACE* cover similar energy and elemental ranges making them particularly suitable for longitude studies (Stone et al. 1998b; Luhmann et al. 2008). The occurrence of the 2006 December SEP events while the *STEREO* spacecraft were still near the Earth allowed the *STEREO* and *ACE* SEP instrumentation to be cross-calibrated (Cohen et al. 2008) providing confidence in future quantitative comparisons.

We examined monthly plots of oxygen intensities as measured by SIS and LET to select multi-spacecraft SEP events (Figure 1). Although no lower limit to the intensities was set for selection, the smallest event chosen had a 10 MeV n^{-1} oxygen event-integrated fluence of 0.3 (cm^2 sr MeV n^{-1})$^{-1}$. For each event, start and stop times were determined for each spacecraft separately and then the intensities of H, He, O, and Fe were integrated over time to create fluence spectra. Although the spectra generally extended from 0.1 to >10 MeV n^{-1}, instead of trying to characterize the entire spectrum at each spacecraft in each event, we extracted fluences at three distinct energies: 0.3, 1, and 10 MeV n^{-1}. The value of 0.3 MeV n^{-1} was selected instead of 0.1 MeV n^{-1} because 0.1 MeV n^{-1} is close to the

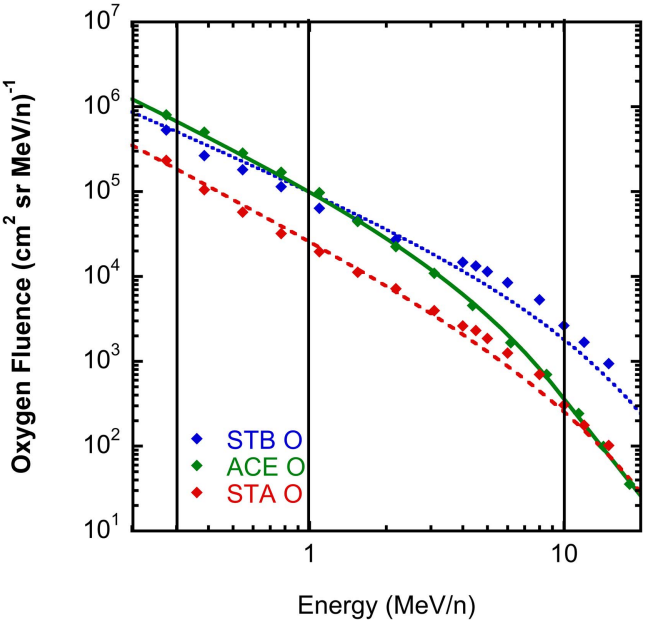

Figure 2. Event-integrated oxygen spectra from *STB*, *ACE*, and *STA* for the 2014/056 three-spacecraft event. Statistical uncertainties are plotted but generally smaller than the data points. Band fits are given by the solid curves. The vertical black lines indicate the three energies studied.

lower energy limit of the ULEIS instrumental capabilities for heavy ions and the detection efficiency is reduced.

Two methods were employed to extract fluences at the three selected energies. The spectra were fit with the Band function (Band et al. 1993), which has often been fit to SEP events with success (e.g., Mewaldt et al. 2012; Desai et al. 2016), to limit the effect of small instrumental and statistical variations that can be present in measured spectra (Figure 2). The fluence values were also determined from data interpolation, assuming a local power law. Generally, the fluence values at the three energies obtained from the fit and interpolation methods agreed within $\leqslant 10\%$. The fits were particularly useful for the Fe spectra obtained from the ULEIS+SIS data because there is a measurement gap between $\sim$2 and 13 MeV n^{-1} due to the different techniques employed by the two sensors. The fluence values used in this study are mostly those extracted from the fits; however, there were a few spectra that were not well represented by the Band fit (e.g., *STB* in Figure 2). For those events and energies, the interpolated values are used.

The solar source region and associated solar events were determined for each SEP event. Radio and electron data from *Wind* (radio), *ACE* (electrons), and *STEREO* were used to help identify the timing of the associated solar event. Solar data from *STEREO*/SECCHI, *SOHO*/LASCO, and *SDO*/AIA were then examined to determine the associated active regions, flares, and CMEs; specific parameters were obtained from various publicly available solar data lists: SolarMonitor, SolarSoft, and the LASCO and CACTus CME catalogs. As the selected events were generally large SEP events, the identification of the solar source was not difficult and several of the events have been identified and studied previously (e.g., Mewaldt et al. 2013; Cohen et al. 2014b; Richardson et al. 2014). For regions visible to near-Earth imaging spacecraft (e.g., *SDO* and *SOHO*), the location of the associated flare was typically provided in various publicly available lists. For backside sources, the location of the flare was estimated from SECCHI movies and images and compared to values determined by others such as N. Nitta (http://www.lmsal.com/nitta/movies/flares_euvi/index.html).

To determine the magnetic footpoint of each spacecraft at the Sun, we utilized the spacecraft mapping tool available at the Predictive Science website (http://www.predsci.com/stereo/spacecraft_mapping.php and http://www.predsci.com/hmi/spacecraft_mapping.php). This tool uses the known locations of the spacecraft and measured solar wind speed (when available; 450 km s^{-1} is assumed when measurements are not available) to ballistically map the field line back to 30 R_S. From there the magnetohydrodynamic coronal field model, MAS (Magnetohydrodynamic Algorithm outside a Sphere; Linker et al. 1999), is used to determine the magnetic field line connection to the photosphere. The longitude difference between the identified associated flare location and the spacecraft magnetic footpoint at the photosphere (calculated for the hour before the flare) was calculated for the observing spacecraft in each event.

Table 1 lists the 41 selected events, their relevant solar parameters, the position of the two *STEREO* spacecraft, and the magnetic footpoints of the observing spacecraft. Events that were observed in heavy ions by both *STEREOs* and *ACE* are identified with bold type. Events that were observed in protons by both *STEREOs* and near-Earth spacecraft (but not in heavy ions) are indicated by italics. During events 2012/148 and 2012/205 the *STEREO-A* (*STA*)/SIT instrument was saturated preventing He, O, and Fe measurements at 0.3 and 1 MeV n^{-1} to be made. Thus, although these events were technically three-spacecraft events, they have been analyzed as two-spacecraft events. Similarly *STEREO-B* (*STB*)/SIT was saturated during the two-spacecraft event of 2014/244; it has not been included in our study. The 2011/066 event was a three-spacecraft event; however, after more closely examining the solar activity associated with this event, it is clear that two well-separated active regions generated large flares at similar times. It appears that the SEP event observed by *STB* may have a different origin than that observed by *ACE* and *STA*. Thus we have removed 2011/066 as a three-spacecraft event.

2.2. Longitudinal Distributions of Two-spacecraft Events

For the two-spacecraft events, we have fit periodic Gaussians of the form

$$j = A\left[\exp\left(-\frac{(x-x0)^2}{2w^2}\right) + \exp\left(-\frac{(x-x0-360)^2}{2w^2}\right) + \exp\left(-\frac{(x-x0+360)^2}{2w^2}\right)\right]$$

to the aggregate distributions for each ion (H, He, O, and Fe) at 0.3, 1, and 10 MeV n^{-1} (Figure 3; fits are indicated by the thick curves), where j is the event-integrated fluence and x is the flare longitude—the spacecraft footpoint longitude; the resulting centers ($x0$) and widths (w) are given in Table 2. A periodic Gaussian was used to account for the possibility that particles may contribute to the measured fluence by traveling either east or west from the center of the distribution. Although the assumption of a Gaussian distribution is likely to be an over-simplification (see, e.g., Giacalone & Jokipii 2012), with only two or three

Table 1
List of Selected Events

Event Year/doy	Event Date	Flare Time[a]	Flare Size	Flare Location[b]	*STEREO* Locations[c] (°)		Observing S/C Δ longitude[d] (°)		
					STB	*STA*	*STB*	*ACE*	*STA*
2011/046	Feb 15	0144	X2.2	S20W10	−94	⋯	42	−41	⋯
2011/066	Mar 7	1943	M3.7	N30W48	−95	88	85	6	−58
2011/080	Mar 21	(0215)	⋯	W128	⋯	88	⋯	64	−30
2011/216	*Aug 4*	*0341*	*M9.3*	*N15W38*	⋯	*101*	⋯	*−15*	*−94*
2011/265	**Sep 22**	**1029**	**X1.4**	**N13E78**	**−97**	**104**	**−29**	**−137**	**121**
2011/295	*Oct 22*	*0918*	*M1.3*	*N27W87*	⋯	*105*	⋯	*−1*	*−78*
2011/308	**Nov 4**	**2328p**	⋯	**N15E150**	**−102**	**105**	**−98**	**131**	**44**
2011/330	*Nov 26*	*609*	*C1.2*	*N11W47*	⋯	*105*	⋯	*15*	*−142*
2012/023	**Jan 23**	**338**	**M8.7**	**N33W21**	**−114**	**108**	**98**	**−13**	**−148**
2012/027	**Jan 27**	**1737**	**X1.7**	**N27W81**	**−114**	**108**	**148**	**64**	**−92**
2012/064	*Mar 4*	*1029*	*M2.0*	*N16E65*	−117	⋯	9	−124	⋯
2012/067	**Mar 7**	**0002**	**X5.4**	**N18E31**	**−118**	**109**	**5**	**−108**	**148**
2012/138	*May 17*	*0125*	*M5.1*	*N11W76*	⋯	115	⋯	*25*	*−39*
2012/147	*May 26*	*(2045p)*	⋯	*W120*	*−117*	⋯	*−140*	*42*	⋯
2012/180	Jun 28	1607	M2.4	N16E46	−116	119	−339	⋯	146
2012/194	Jul 12	1537	X1.4	S13W03	−115	⋯	20	−23	⋯
2012/205	*Jul 23*	*0200*	⋯	*W140*	*−115*	⋯	*−153*	*100*	⋯
2012/244	*Aug 31*	*2000*	*C8.4*	*S23E47*	*−116*	⋯	*−11*	*−112*	⋯
2012/263	Sep 19	(1200)	⋯	E159	−117	125	−123	⋯	39
2012/313	Nov 8	0208	M1.7	N31E89	−123	127	−48	⋯	79
2013/064	Mar 5	(0330)	⋯	E135	−140	131	−64	⋯	4
2013/074	Mar 15	0546	M1.1	N09E06	−140	⋯	79	−65	⋯
2013/101	*Apr 11*	*0655*	*M6.5*	*N07E13*	*−142*	⋯	*75*	*−75*	⋯
2013/133	*May 13*	*1548*	*X2.8*	*N08E89*	*−142*	⋯	*29*	*202*	⋯
2013/142	*May 22*	*1308*	*M5.0*	*N14W72*	⋯	*137*	⋯	*36*	*−136*
2013/172	*Jun 21*	*0230*	*M2.9*	*S14E76*	*−140*	⋯	*4*	*−103*	⋯
2013/231	**Aug 19**	**(2300)**	⋯	**W175**	**−138**	**144**	**−62**	**113**	**−15**
2013/278	Oct 5	(0700)	⋯	E117	−140	147	−31	⋯	33
2013/284	Oct 11	0701	M1.5	N21E87	−140	147	−12	⋯	73
2013/306	Nov 2	(0430)	⋯	W127	−143	148	−150	⋯	−70
2013/307	Nov 4	(0500)	⋯	W168	−143	149	−117	⋯	−52
2013/311	Nov 7	2335p	M1.8	S09W98	−144	149	−153	⋯	−90
2013/347	**Dec 13**	**(2000)**	⋯	**E155**	**−149**	**150**	**−58**	**148**	**−13**
2013/360	**Dec 26**	**(0300)**	⋯	**E160**	**−151**	**151**	**−11**	**114**	**−5**
2014/008	**Jan 8**	**1804**	**X1.2**	**S12W08**	**−153**	**151**	**45**	**−4**	**178**
2014/021	Jan 21	(2100)	⋯	E165	−155	151	−71	⋯	−2
2014/052	Feb 21	(1530)	⋯	E120	−160	152	−3	⋯	43
2014/056	**Feb 25**	**0039**	**X4.9**	**S12E77**	**−160**	**153**	**41**	**−126**	**47**
2014/157	Jun 6	(1300)	⋯	E140	−165	160	−41	⋯	7
2014/161	Jun 10	1236 1136	X1.5 X2.2	S19E81	−164	160	10	⋯	68
2014/180	Jun 29	(1200)	⋯	E140	−163	162	−44	⋯	−39

Notes. Bold type indicates three-spacecraft events in heavy ions.
Italic type indicates three-spacecraft events in protons but not heavy ions.
[a] Parenthetical values indicate times estimated to the nearest 15 minutes from the associated type III radio burst (https://swaves.gsfc.nasa.gov/cgi-bin/wimp.py) for flares not visible from L1/Earth. Times with "p" are for the previous day.
[b] Locations are relative to the Earth–Sun line (i.e., solar central meridian as viewed from Earth).
[c] Spacecraft longitude relative to the Earth–Sun line. Ellipses indicate that the spacecraft did not register the event in 10 MeV n^{-1} oxygen.
[d] Longitude difference between the flare and the spacecraft magnetic footpoint at the photosphere. Ellipses indicate that the spacecraft did not register the event in 10 MeV n^{-1} oxygen.

measurements in each event and large event-to-event variability, we cannot justify investigating more complicated distributions.

Ideally, when fitting an aggregate of distributions we would normalize the individual distributions by their amplitude and align their centers before fitting. However, with only two measurements in each event, this is not possible. The same two measurements could be equally representative of a low-amplitude, wide distribution, and a high-amplitude, narrow distribution. Lario et al. (2013, 2006) partially addressed this by assuming the center of the distribution was the same in all events and fitting the ratio of the measured fluences to remove the variation in distribution amplitudes. We have applied this method to our group of two-spacecraft events to determine centers and widths for each ion at the three energies. However, we found that a single center was not consistent with all the events in that no matter what center value was used, some

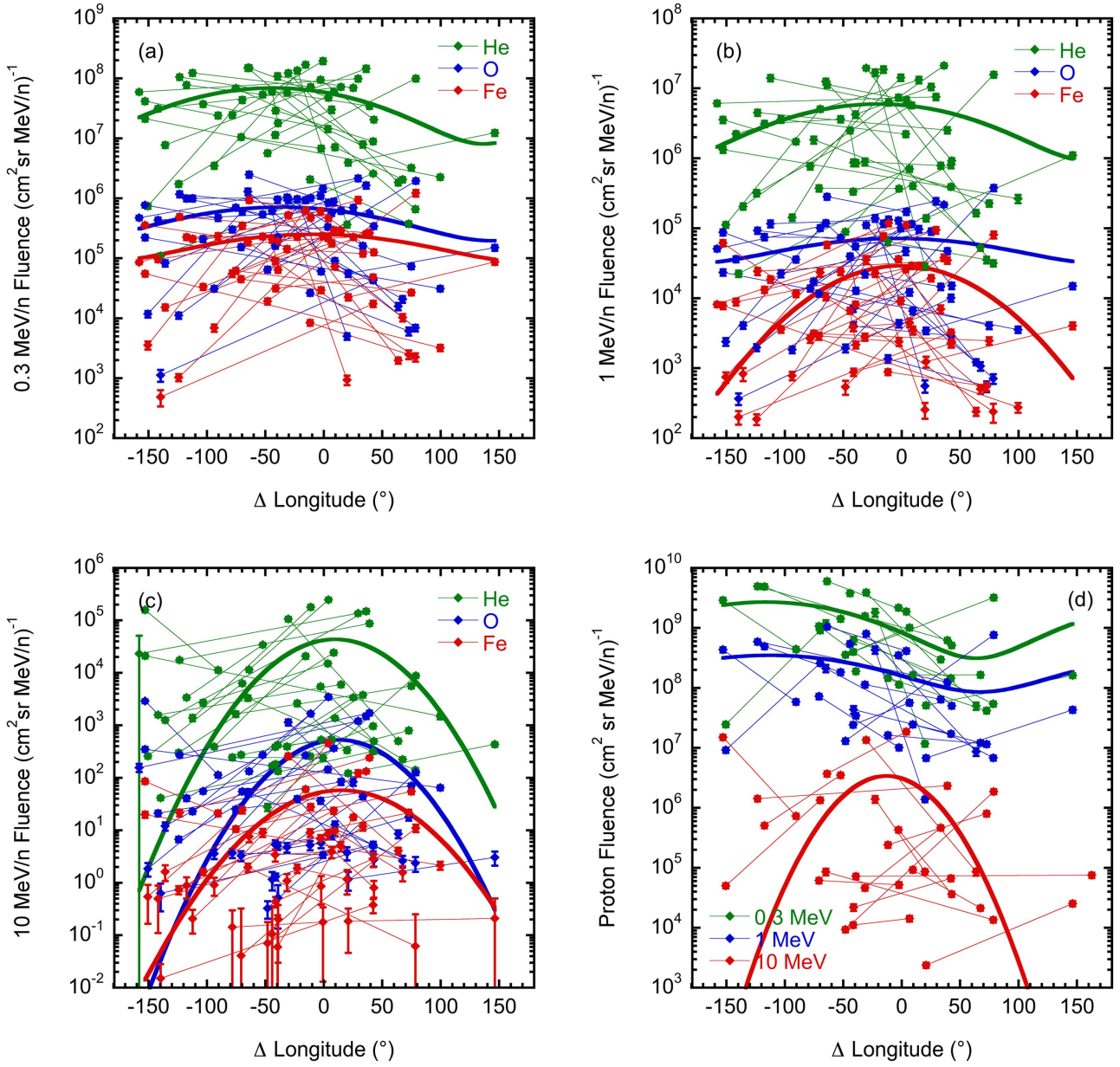

Figure 3. Periodic Gaussian fits (indicated by the thick curves) to the two-spacecraft events for He, O, and Fe at (a) 0.3, (b) 1, and (c) 10 MeV n^{-1}; protons at all three energies are in panel (d). Individual events are connected by lines. Note that there were fewer two-spacecraft events measured in H (i.e., more events were three-spacecraft events). Δ Longitude values are calculated as flare-spacecraft footpoints, thus negative values correspond to footpoints west of the flare location, and positive values correspond to locations east of the flare.

Table 2
Centers and Widths for Two-spacecraft Periodic Gaussian Fits By Element and Energy

Elemt	Centers (°)			Widths (°)		
	0.3 MeV n^{-1}	1 MeV n^{-1}	10 MeV n^{-1}	0.3 MeV n^{-1}	1 MeV n^{-1}	10 MeV n^{-1}
H	−120 ± 23	−110 ± 36	−13 ± 18	75 ± 16	88 ± 21	30 ± 20
He	−43 ± 15	−20 ± 23	9.7 ± 15	75 ± 17	80 ± 24	36 ± 15
O	−37 ± 22	−3.8 ± 44	13 ± 17	90 ± 22	100 ± 31	35 ± 17
Fe	−9.1 ± 34	−0.47 ± 16	15 ± 19	97 ± 28	54 ± 18	41 ± 19

events had higher fluences measured by the spacecraft with larger longitude difference (relative to the flare location). Another drawback to the Lario et al. method is that, unlike the periodic Gaussian, it does not allow for particles to travel both eastward and westward from the distribution center to contribute to the observed fluence. A comparison of the centers and widths resulting from the two methods for He, O, and Fe in the two-spacecraft events is given in Figure 4. The centers

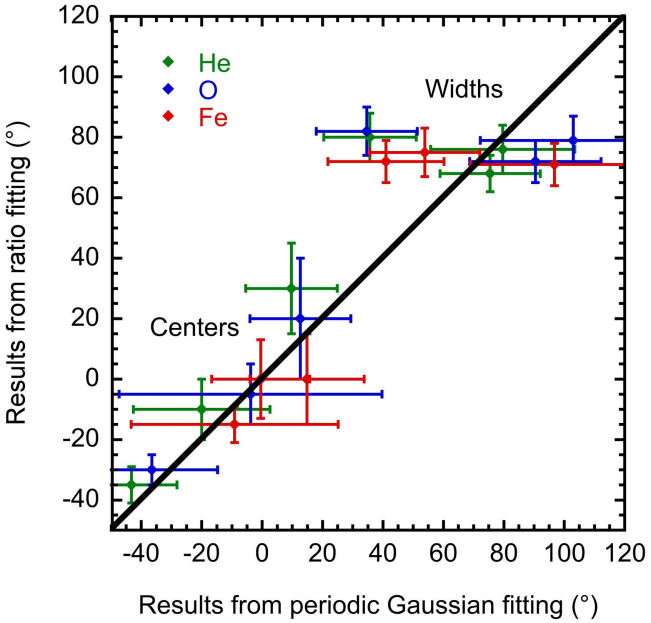

Figure 4. Comparison of the center and width values obtained from fitting a periodic Gaussian to the two-spacecraft events (e.g., Figure 3) and from the normalization method of Lario et al. (2006).

show reasonable agreement between the two methods, but the width values show significant discrepancies. For the remainder of this paper, we have used the periodic Gaussian fit results.

Figure 5 shows the widths and centers as a function of energy for each element as well as the average over the elemental results. With the exception of H center values at 0.3 and 1 MeV n^{-1}, there does not appear to be a strong elemental dependence on the widths or centers. While the widths of the distributions are similar at 0.3 and 1 MeV n^{-1}, they narrow significantly at 10 MeV n^{-1} (though this is not the case for the widths resulting from the Lario et al. method, see Figure 4). Most of the center values are negative, indicating the particle source center is westward of the flare location, though there is a suggestion of a shifting of the centers toward 0° (i.e., direct-flare connection) with increasing energy (however, the uncertainties in the He, O, and Fe values nearly overlap). It is unclear why the H centers at 0.3 and 1 MeV n^{-1} are signficantly farther west (more negative) than the heavy ions, but it is also apparent in Figure 3. It should be noted that more of the selected events were three-spacecraft events in protons, leaving fewer two-spacecraft events for the H aggregate fitting relative to that of He, O, and Fe. It is possible that this causes the negative-longitude portion (i.e., left side) of the plot in Figure 3(d) to be less populated, which then skews the fit.

2.3. Longitudinal Distributions of Three-spacecraft Events

We have heavy ion fluence measurements from all three spacecraft in 10 events allowing us to examine the longitudinal distribution directly. For these, we have calculated the amplitude, width, and center of the periodic Gaussian, which passes through all three points (e.g., Figure 6). Becuase these are calculated values rather than true fits to the data, no uncertainties are obtained. As with the aggregate fits, these calculations were made for H, He, O, and Fe at 0.3, 1, and 10 MeV n^{-1}, resulting in 12 individual Gaussians per event; the resulting centers and widths are given in Table 3. Plots similar to Figure 5 using the average of the results from the three-spacecraft events are given in Figure 7. Any energy dependence of the average centers determined from the three-spacecraft events is slight (and no energy dependence is consistent with the uncertainties), contrary to the aggregate results. The energy dependence in the average widths is still apparent, though to a smaller degree.

With the three-spacecraft events, we can examine event-to-event variability in the longitudinal distributions. Figure 8 shows the centers and widths for each event as a function of energy and Figure 9 shows the values versus Q/M. We have no direct measurement of the charge states of the elements and so have assumed values of 1, 2, 7, and 15 for H, He, O, and Fe (respectively, corresponding to Q/M values of 1, 0.5, 0.44, and 0.27). The assumptions for O and Fe were taken from Luhn et al. (1985), but are not overly critical to the interpretation of the data as only general trends with Q/M are sought. As can be seen, there is significant variability in the widths and centers from event to event, though the fact that most of the lines are parallel suggests that the general trend with energy or Q/M is similar in many events.

To remove the variability, we have normalized the widths and calculated the centers relative to their values at 0.3 MeV n^{-1} and replotted the data versus energy (Figure 10). Similarly, we use the values at Q/M = 1 for normalization in Figure 11. The trend of decreasing width with increasing energy is quite clear, whereas the shift in center is more subtle. The Fe widths appear to be narrower than for H, suggesting a possible Q/M dependence; however, the He and O values do not appear to be significantly different from those of H. No clear Q/M dependence in the centers is evident. The 10 MeV n^{-1} outlier curve is event 2013/360. In this event the *STB* fluences were all lower than those of *STA* for He, O, and Fe, but for protons *STB* fluences were higher than at *STA*. Because of the small separation between the two *STEREO* spacecraft at this time, the differences in fluence have dramatic effects on the calculated distribution. In this case, the center of the H distribution is calculated to be ~100–120° removed from those of the heavy ions. In fact, at 0.3 and 1 MeV n^{-1}, it was not possible to calculate a periodic Gaussian that was consistent with the measured H fluences.

For the two-spacecraft events, it is not possible to make individual event calculations for the Gaussian parameters without assuming a value for either the amplitude, center, or width. Given the variability of the parameters deteremined from the three-spacecraft events, it was not clear what value to assume for any of the parameters that would yield useful information on the remaining ones for a given two-spacecraft event. However, 12 of the heavy ion two-spacecraft events were three-spacecraft events in protons (as indicated with italics in Table 1). For these events, we assumed the center of the distribution calculated from the proton fluences was the same for the heavy ions and calculated the amplitudes and widths accordingly when possible (some events had fluences measured at the two spacecraft, which were not consistent with the assumed center). In an effort to account for uncertainty in how well the H centers match those of the heavy ions, the calculations were performed for centers shifted by ±10° from the H centers as well. Figure 12 shows the average widths as a function of energy for both the two-spacecraft and three-spacecraft events. Although there is more variability and larger uncertainties in the two-spacecraft results, they are generally

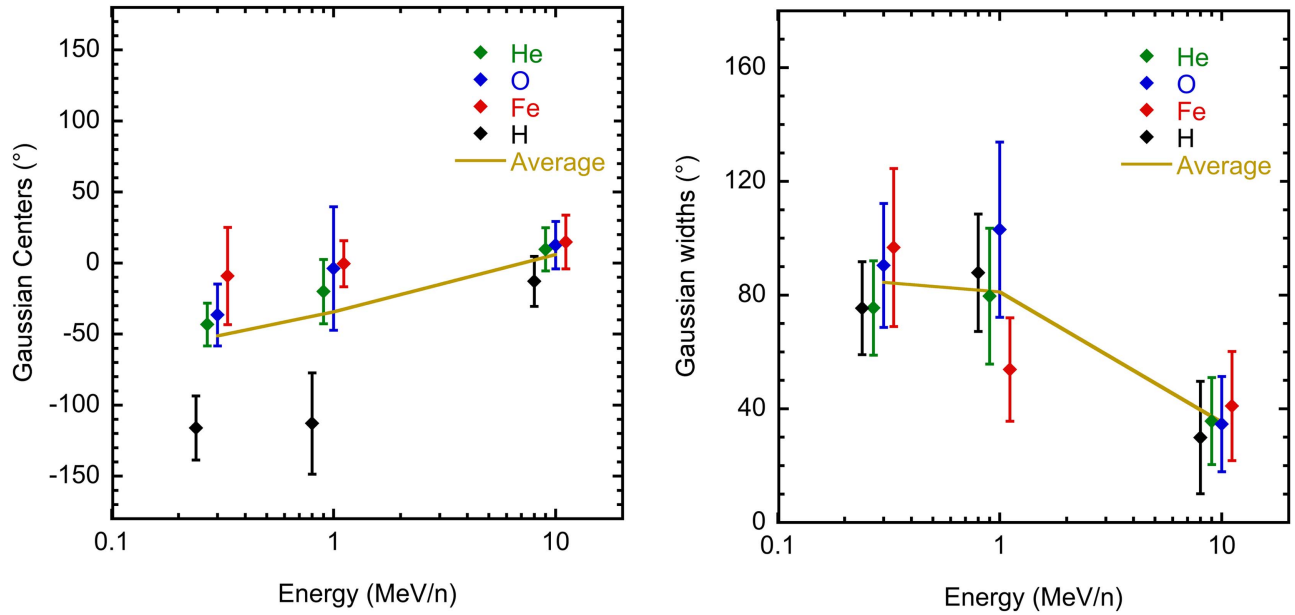

Figure 5. Gaussian centers (left) and widths (right) obtained from the aggregate fits of each element as a function of energy. Symbols for each element are slightly shifted relative to each other in energy to more easily distinguish the values at 0.3, 1, and 10 MeV n^{-1}.

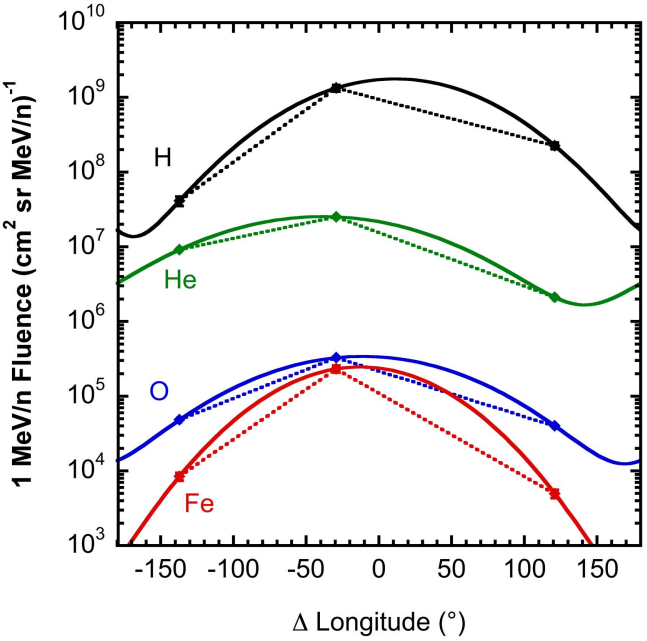

Figure 6. 1 MeV n^{-1} event-integrated fluences of H, He, O, and Fe for the 2011/265 event measured by *STB* (−29°), *ACE* (−137°), and *STA* (121°) as a function of the longitude difference between the flare location and spacecraft magnetic footpoint at the photosphere. The curves correspond to periodic Gaussian distributions calculated to pass through the points.

consistent with the three-spacecraft values and show the same trend with energy.

3. Discussion

The 0.3 and 1 MeV n^{-1} widths obtained for all species from the aggregate fits to two-spacecraft events are significantly larger than what has been obtained in previous studies for protons at higher energies. Statistical studies have been primarily focused on protons and electrons (Lario et al.2006, 2013, Richardson et al. 2014) and this study addresses heavy ions. However, we obtain similarly larger widths for protons. It should be noted that the Lario et al. (2014) and Richardson et al. (2014) surveys used peak intensities whereas we have used event fluences. Although it is possible that this difference could result in significantly different derived distribution widths, Lario et al. (2006) analyzed both peak intensities and fluences of 4–13 MeV n^{-1} and 27–37 MeV n^{-1} protons and found little to no difference in the derived widths.

One explanation for the wider distribution is the event-to-event variability in the size and center of the distributions. When the events are fit together without shifting each event to align the centers, the resulting aggregate distribution can appear artificially wide. Similarly, without normalizing the measurements by the distribution amplitude, the combined distribution may not be representative of what is "typical" for an individual event. A comparison of Figures 5 and 7 supports this (note the different *y*-axis scales); the average width values at 0.3 and 1 MeV n^{-1} obtained from the three-spacecraft calculations are substantially lower than those from the aggregate two-spacecraft fits (this is true regardless of the method used for fitting the two-spacecraft events). Interestingly, the values at 10 MeV n^{-1} are roughly consistent for the periodic Gaussian method, suggesting that the event-to-event variability in the two-spacecraft events is less; though this does not appear to be the case for the three-spacecraft events (e.g., Figure 8). The three-spacecraft values, ranging from 36° to 52°, are more consistent with widths obtained in previous studies, e.g., 43° ± 2° (Lario et al. 2013), 43° ± 13° (Richardson et al. 2014), and 36° ± 2° (Lario et al. 2006). The Richardson et al. value is derived from the average of individual three-spacecraft caculations similar to what was done here; however, the Lario et al. 2013 and 2006 values include both two- and three-spacecraft events. Although the aggregate fitting approach of Lario et al., discussed previously, effectively removes the variation in amplitude from event to event, it does not account for event-to-event variation in the centers of the distribution and one might expect some artificial widening. However, Lario

Table 3
Periodic Gaussian Centers and Widths for Three-spacecraft Events

Event	Elmnt	Centers (°)			Widths (°)		
		0.3 MeV n^{-1}	1 MeV n^{-1}	10 MeV n^{-1}	0.3 MeV n^{-1}	1 MeV n^{-1}	10 MeV n^{-1}
2011/265	H	20	11	−12	58	54	40
	He	−27	−39	−15	83	69	39
	O	−2.7	−11	−19	79	64	41
	Fe	4.2	−13	−14	59	48	42
2011/308	H	−36	−21	14	46	44	44
	He	−33	−16	8.7	50	51	40
	O	−21	−19	15	42	46	42
	Fe	−11	−9.6	20	40	45	41
2012/023	H	−51	−38	−29	60	56	46
	He	−33	−25	−23	56	47	45
	O	−23	−21	−23	67	53	45
	Fe	−32	−22	−27	63	51	46
2012/027	H	−54	−36	−18	56	49	45
	He	−20	−8.7	−19	53	40	45
	O	−33	−25	−11	50	48	45
	Fe	−40	−25	−12	47	45	41
2012/067	H	−33	−57	−76	58	56	50
	He	−67	−78	−71	46	43	53
	O	−69	−71	−68	74	46	54
	Fe	−46	−66	−66	54	54	54
2013/231	H	−28	−9.5	4.6	44	37	28
	He	−24	1.2	…	49	36	…
	O	−11	0.58	−4.7	39	32	29
	Fe	−2.7	2.7	…	33	28	…
2013/347	H	110	100	69	59	53	35
	He	110	97	49	48	45	32
	O	120	89	50	57	54	30
	Fe	74	60	53	40	37	27
2013/360	H	…	…	−81	…	…	52
	He	−98	−45	24	38	50	30
	O	−65	−67	39	50	48	22
	Fe	−57	−68	39	50	50	22
2014/008	H	−92	−87	−81	43	39	33
	He	−81	−79	−75	35	30	31
	O	−82	−80	−72	35	32	32
	Fe	−83	−79	−69	34	31	32
2014/056	H	−42	−42	−40	23	24	21
	He	−53	−46	−40	32	22	17
	O	−44	−45	−39	26	29	19
	Fe	−40	−40	−40	22	19	16

et al. (2013) examined >15 MeV protons in their studies, not the ⩽1 MeV energies for which we found artificially wide distributions in the aggregate fits, which may explain why their derived widths are similar to our 10 MeV n^{-1} two-spacecraft values.

Although there is significant event-to-event variation, the Gaussian widths derived from the three-spacecraft events clearly show a trend of decreasing with increasing energy. Although less definitive due to the small sample size, the same result was obtained by Cohen et al. (2014b) in a study of five large SEP events. It is possible that at lower energies there are contributions from other energetic particle sources (e.g., small, unidentified SEP events, particles accelerated at shocks associated with co-rotating interaction regions), which are absent (or significantly smaller) at higher energies. Although we cannot rule this possibility out, the energy dependence of the distribution widths can also be explained by several acceleration and/or transport related phenomena.

As the strength of the shock generally decreases with distance from the Sun, the maximum energy to which the shock can accelerate ions also decreases (Li et al. 2005; Zank et al. 2007); thus, higher energy ions are accelerated over a shorter time and distance than lower energy ions. As the shock and associated CME move outward from the Sun they may expand laterally, intersecting a broader longitudinal range of field lines (de Lucas et al. 2011). This could allow the lower energy ions access to a wider distribution of field lines than the high energy ions.

It has also been suggested that the high energy ions are predominantly accelerated near the nose of the shock where the shock is strongest (Dalla et al. 2017), while the lower energy ions are accelerated over a broader expanse of the shock. This will also lead to lower energy ions being injected onto field lines covering a broader range of longitudes. However, there are some theories that the higher energy ions are not accelerated at the nose but rather at the flanks of the shock (Kahler 2016). If the acceleration is occurring equally at both

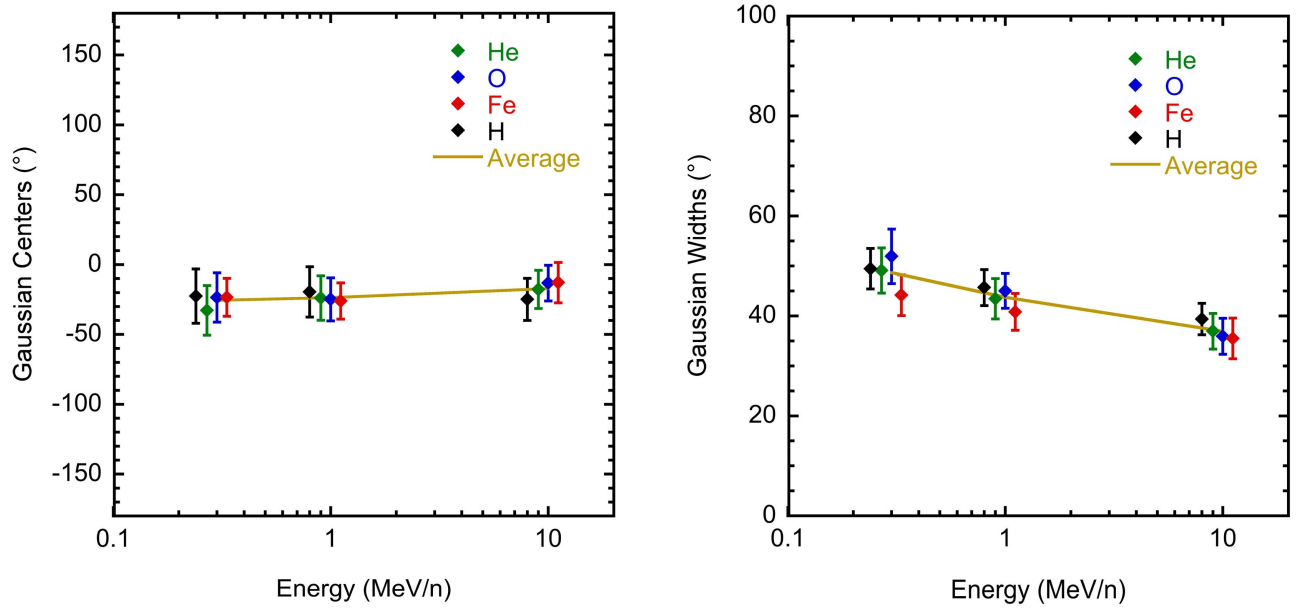

Figure 7. Average Gaussian centers and widths for individual three-spacecraft calculations for each element as a function of energy. Symbols for each element are slightly shifted relative to each other in energy to more easily distinguish the values at 0.3, 1, and 10 MeV n^{-1}.

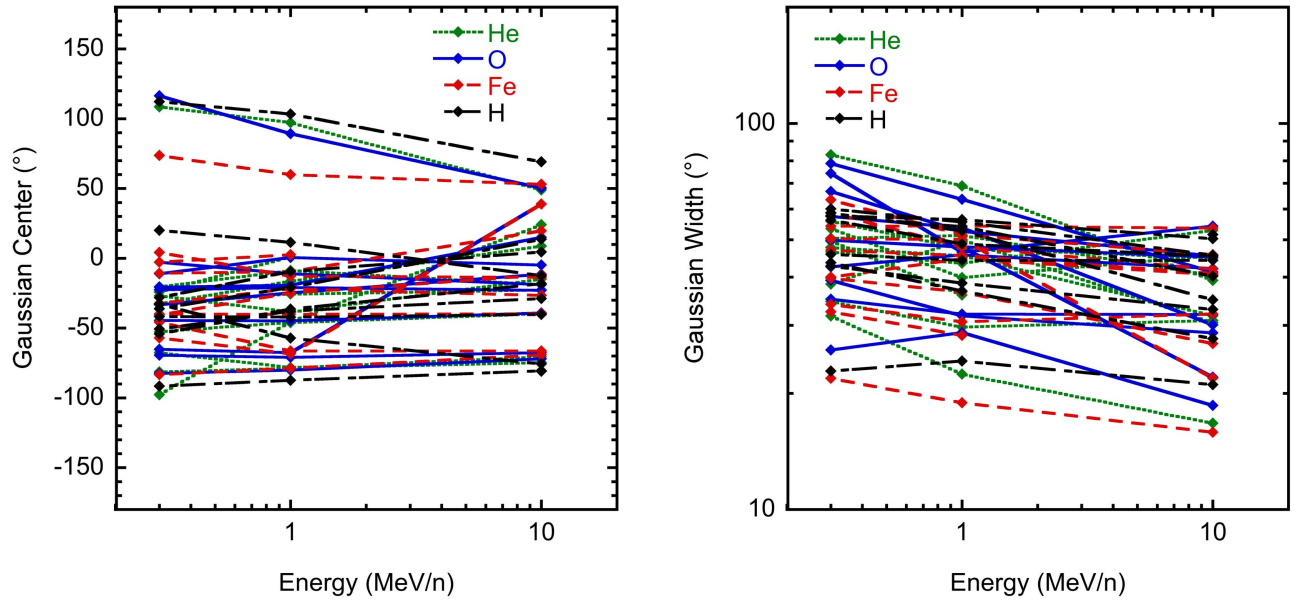

Figure 8. Individual Gaussian centers and widths for three-spacecraft events as a function of energy. Lines connect the values from each event for each element.

flanks, fitting the resulting distribution at 1 au to a single Gaussian would likely yield a similar width (or possibly wider) to that obtained for the lower energy ions. If the acceleration is occurring primarily at one flank and not the other, then we would expect not only a narrower distribution of the high energy ions, but also a significant shift in the center of the distribution relative to that of the lower energy ions, which is not evident. In either case, the different time history of the high- and low-energy ions may remain.

Finally, with time, field lines are believed to co-rotate in longitude (Giacalone & Jokipii 2001, 2012). Slower ions will experience more of this because their travel time to 1 *au* can be significantly longer than that of the faster (higher energy) ions. This may also play a role in observing lower energy ions over a wider longitudinal range.

Given that acceleration and transport processes are often dependent on a particle's rigidity (e.g., Ng et al. 2003; Lee 2005), we expected that the widths of the Gaussian distributions would depend on Q/M, but there is no strong trend with Q/M apparent in our results. In order to investigate this further, we attempted to remove the energy dependence in the calculated widths. We fit the average width values versus energy (Figure 7) with a power law and normalized the individual calculated widths according to energy. Histograms were then made of the normalized widths for each element (Figure 13). Because the energy dependence has been removed, each histogram contains widths from all energies in the three-spacecraft events. The widths of the H, He, O, and Fe distributions exhibit no significant trend, as indicated by the calculated means and standard deviations given in each figure

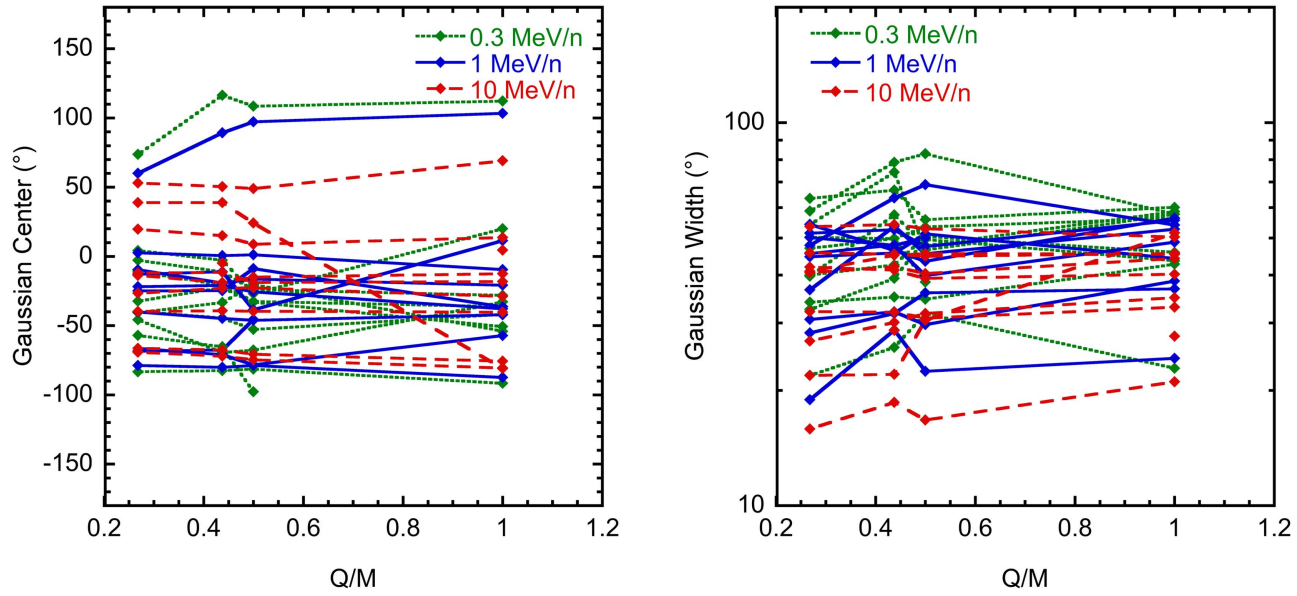

Figure 9. Individual Gaussian centers and widths for three-spacecraft events as a function of element's charge-to-mass (Q/M) ratio. Lines connect the values from each event for each energy.

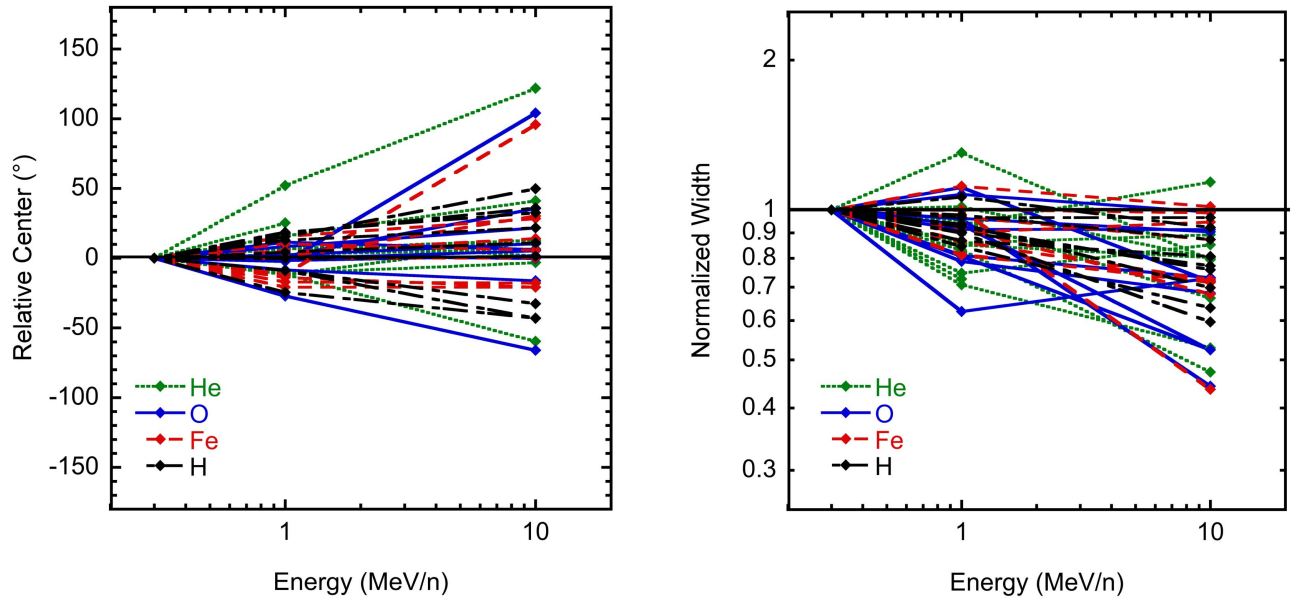

Figure 10. Same data as in Figure 7 but normalized to the value obtained at 0.3 MeV n^{-1}.

panel. Thus, there is no evidence of a substantial Q/M dependence, which, surprisingly, suggests that the processes that dominate the spread of particles in the inner heliosphere during large SEP events are not strongly dependent on particle rigidity. This would be consistent with diffusion being dominated by the movement of field lines rather than the transfer of particles across field lines or consistent with the spreading being governed primarily by the width of the CME-driven shock.

The centers of the derived distributions tend to lie west of the flare (note that the delta longitude values were calculated as flare-footpoint, thus negative (positive) delta longitude values indicate footpoints westward (eastward) of the flare), though there is significant variability. This has been observed by others in previous studies (Lario et al. 2006, 2013). While it would be unexpected if the source region were only the flare, it is understandable in the case of acceleration by CME-driven shocks in the corona. A magnetic field line that connects to a shock at some height above the flare will have a footpoint at the photosphere that will generally be further westward (Lario et al. 2014). As can be seen from Figure 8, the distribution of center values is broad but shifts toward 0° with increasing energy, though a systematic shift is not as clearly reflected in the average values (Figure 7). The mean value for 10 MeV n^{-1} is $-17° \pm 7°$, similar to the $-13° \pm 2°$ obtained for 15–40 and 25–53 MeV protons by Lario et al. (2013), the $-26° \pm 4°$ and $-18° \pm 4°$ for 4–13 and 27–37 MeV protons (respectively) by Lario et al. (2006), and the $-15° \pm 7°$ value obtained by Richardson et al. (2014) for >25 MeV protons. The center values farther west from the flare obtained for the lower energies can be understood in terms of these particles escaping from the acceleration region at higher heights above the flaring

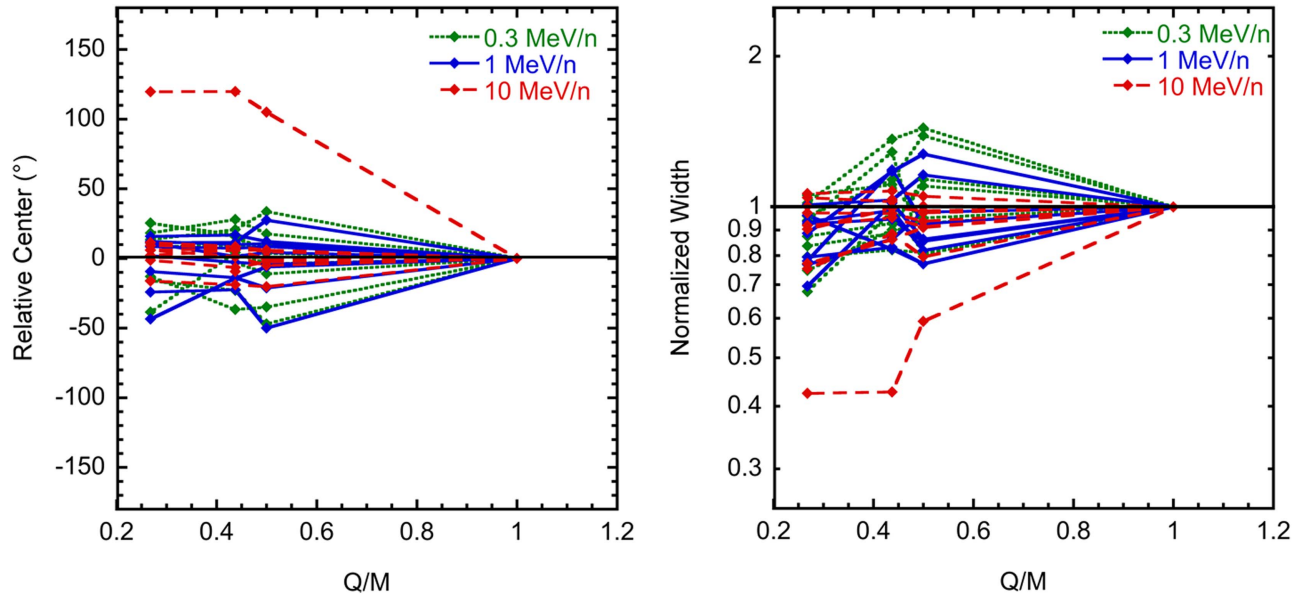

Figure 11. Same data as in Figure 8 but normalized to the value obtained for H.

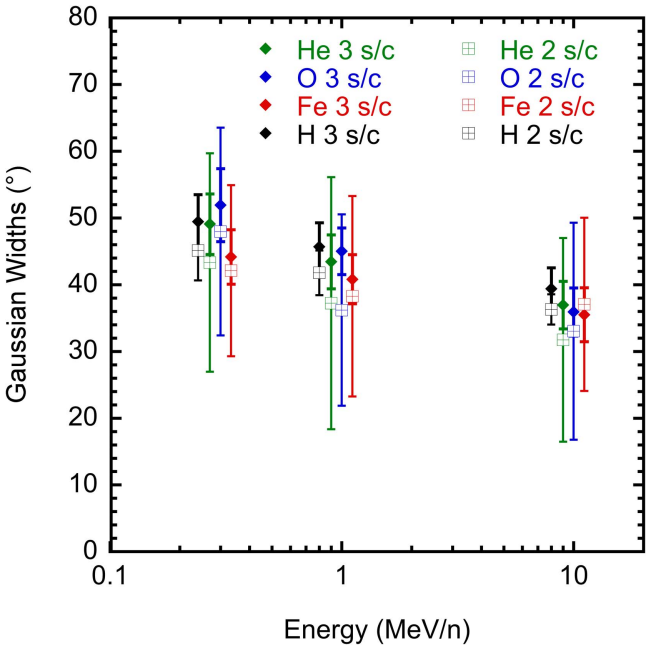

Figure 12. Average widths obtained from three-spacecraft events (closed diamonds) as well as two-spacecraft events that had proton measurements at three spacecraft as a function of energy (open squares). The two-spacecraft uncertainties reflect the uncertainty on individual event calculations based on varying the assumed Gaussian center by ±10°.

region. This is again consistent with the notion that lower energy particles continue to be accelerated and released over larger distances as the CME propagates away from the Sun.

There has been debate over the longitudinal dependence of Fe relative to O in large SEP events with Fe/O ratios significantly higher than the average value of 0.134 (Reames 1998). One proposed scenario suggests that in addition to the shock-accelerated population, there is an SEP component with enhanced Fe/O resulting from flare-related acceleration processes that is more likely to be observed by spacecraft well connected to the flaring region and at higher energies (Cane et al. 2003, 2006). In our survey, four of the three-spacecraft events have Fe/O ratios at 10 MeV n^{-1} greater than 0.3 (>2 times the average value) at one or more of the three spacecraft: 2011/308, 2013/347, 2013/360, and 2014/056. In the direct-flare contribution scenario one would expect a composite longitudinal distribution resulting from a narrow, flare-related distribution and a wider CME-related one. Because the flare-related component would contribute much more strongly to the Fe fluence than to the O fluence, the overall longitude distribution would be expected to be narrower for Fe. Similarly, since the CME-related distribution may have a center offset from the flare location, contrary to that of the flare-related component, one expects the center of the composite Fe distribution to be closer to the flare location (i.e., 0° separation) than that of O.

Figure 14 presents the 10 MeV n^{-1} O and Fe Gaussian parameters as a function of the highest Fe/O ratio measured by the three spacecraft observing the event (note that event 2013/231 did not have a measurable 10 MeV n^{-1} Fe fluence, so it is not included in the figure). The left panel plots the difference of the absolute value of the Fe and O distribution centers; a positive difference value indicates the center of the O distribution was closer to the flare location than that of the Fe distribution, while a negative difference value indicates that the Fe distribution center was closer to the flare. The four events with Fe/O ratios >0.3 do not particularly stand out relative to the other events and all of the events have O and Fe center values quite close to each other (i.e., the differences in their center positions are within ±5°). The right panel of Figure 14 shows the ratio of the Fe and O widths for each event; values <1 indicate events for which the O distribution is wider than that of Fe. Nearly all the events fall within 10% of equal widths and, again, the enhanced Fe/O events do not exhibit significantly different behavior.

We have also examined the Fe/O ratios versus delta longitude. Figure 15 shows the 10 Mev n^{-1} Fe/O ratios versus the longitude separation between the flare and spacecraft footpoint (similar to Figure 3). The left panel shows the two-spacecraft events and their aggregate fit; the right panel shows all three-spacecraft events and the corresponding calculated

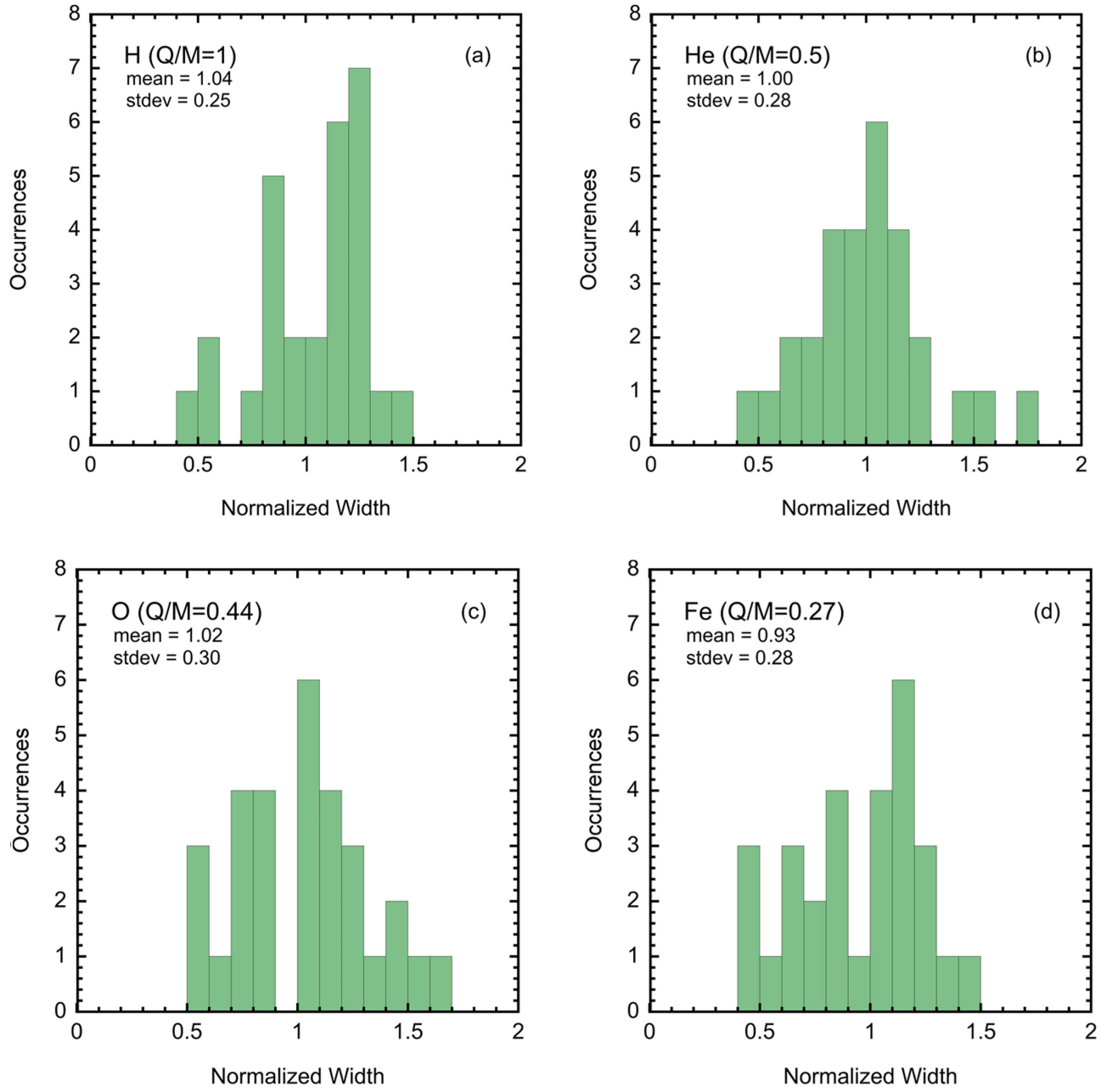

Figure 13. Histograms of the energy-detrended three-spacecraft widths for each element.

Gaussian curves. The distribution determined from the two-spacecraft events is very wide, but not flat, indicating a systematic difference in the O versus Fe longitude distributions. While there does appear to be a peak in the distribution, and the majority of the high Fe/O ratios are at positive values of delta longitude, it is not centered at 0° as would be expected from the direct-flare contribution scenario. The three-spacecraft distributions mostly reflect substantial variability with only one event centered within 20° of direct-flare connection (i.e., delta longitude = 0°). Generally, the Fe/O ratios from the three-spacecraft events show less variability with delta longitude than those from the two-spacecraft events. Thus we do not find support for the direct-flare contribution scenario in either the small sample of three-spacecraft events or the aggregate distribution of the two-spacecraft events.

4. Consideration of Complicating Factors

There are several conditions that could affect the distribution properties that we have determined for the selected multi-spacecraft events. Specifically, we have considered the effects of one or more of the spacecraft being in an interplanetary coronal mass ejection (ICME) during the event unrelated to the source CME; of the presence of a particle reservoir during the event; of the presence of an energetic storm particle (ESP) event at one or more of the spacecraft; and of using the spacecraft footpoint calculated at the photosphere versus higher in the corona. Given the difficulties with two-spacecraft event aggregate fits, we have limited our investigation to three-spacecraft events. Table 4 notes which three-spacecraft events and spacecraft exhibited ICMEs, reservoirs and ESP events.

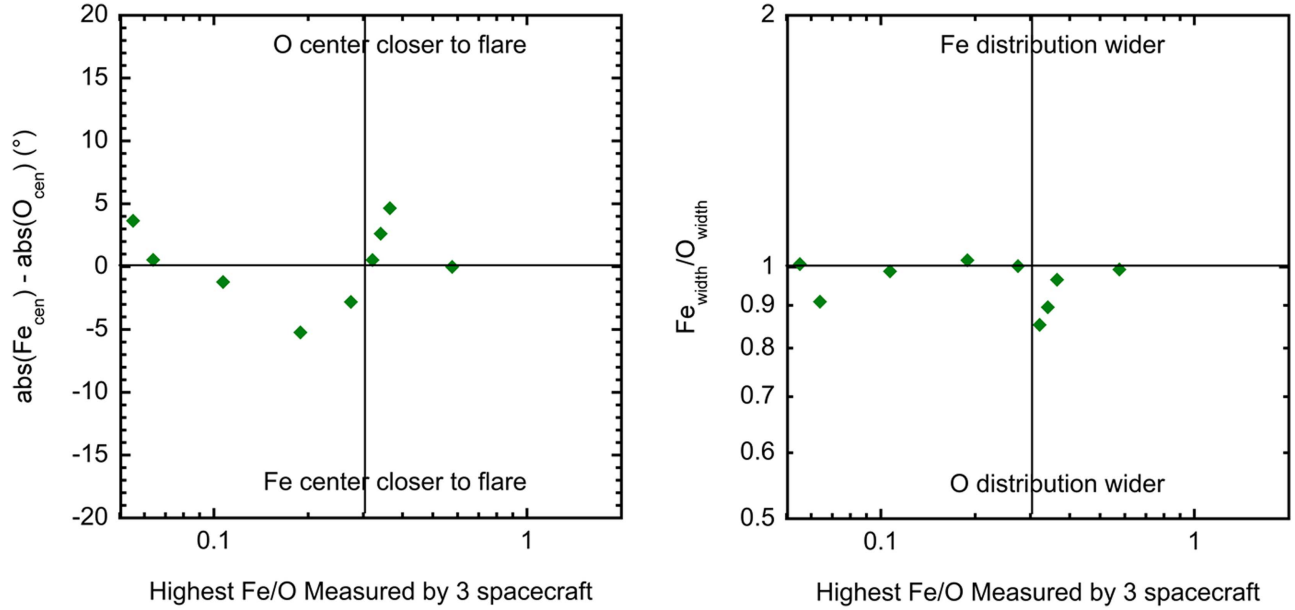

Figure 14. (Left) The difference of Fe and O centers (relative to the flare) vs. the highest Fe/O ratio measured by the three spacecraft at 10 MeV n^{-1} for nine three-spacecraft events. Points in the positive (negative) *y*-axis half have O (Fe) distribution centers closer to the flare. (Right) The ratio of the widths of the Fe and O distributions vs. the highest Fe/O ratio measured. Points below (above) 1 on the *y*-axis have wider O (Fe) distributions. The vertical lines indicate Fe/O = 0.3, which is >2 times the average value.

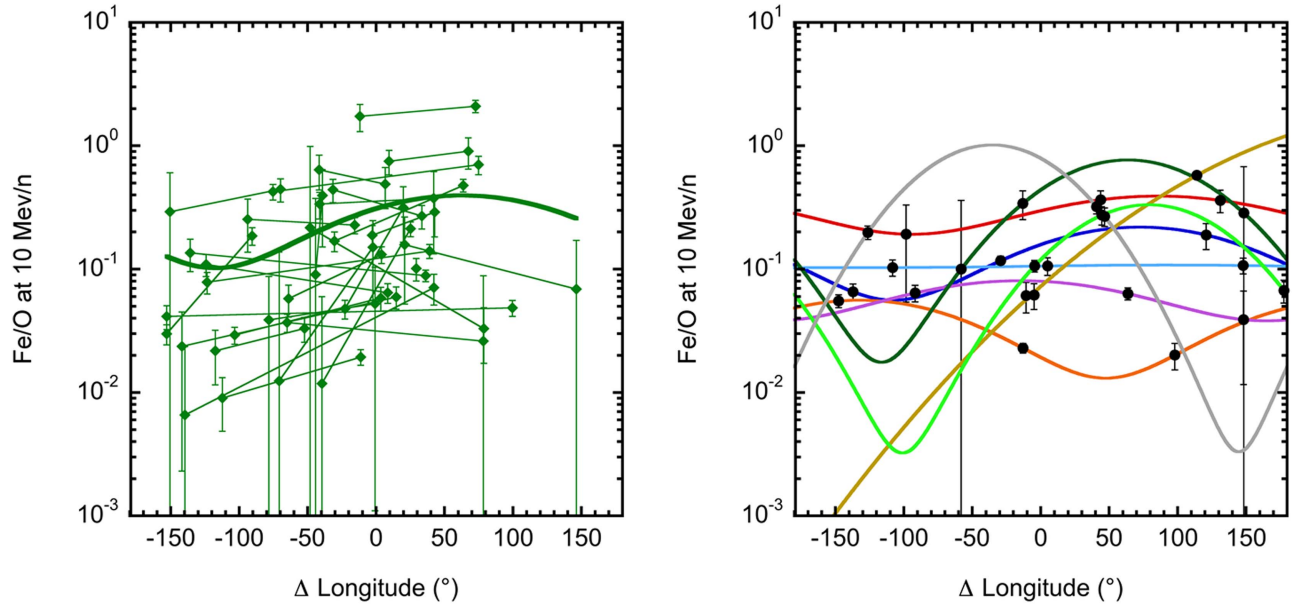

Figure 15. (Left) Fe/O values at 10 Mev n^{-1} for two-spacecraft events vs. delta longitude and the aggregate fit (solid line). (Right) 10 MeV n^{-1}Fe/O values vs. delta longitude for three-spacecraft events and their corresponding Gaussians (solid lines).

4.1. Unrelated Interplanetary Coronal Mass Ejections

We examined the solar wind data as well as the public lists of ICMEs observed by the *ACE* (Richardson and Cane http://www.srl.caltech.edu/ACE/ASC/DATA/ftp/pub/ace/level3/icmetable2.htm) and *STEREO* (Jian www-ssc.igpp.ucla.edu/~jlan/STEREO/Level3/STEREO_Level3_ICME.pdf) spacecraft for four days preceeding and during the time periods of our selected three-spacecraft events. We followed the classification employed by Lario & Karelitz (2014): 0 = no ICME was observed; 1 = an ICME was between the spacecraft and the Sun at the time of the SEP event; 2 = the spacecraft was in the ICME sheath at the onset of the SEP event; 3 = the spacecraft was in the ICME loop at the onset of the SEP event; 4 = the ICME was beyond the spacecraft (requiring the SEP onset to occur within 72 hr of the end of the ICME). Lario and Karelitz found that for 9–15 and 15–40 MeV protons, class 1 events had lower peak intensities while class 3 (followed by class 4) events had the highest proton intensities. They attributed the increased intensities in events of class 3 or 4 to the fact that the disruption in the magnetic field topology caused by the presence of an ICME at or beyond the spacecraft had confined or reflected energetic particles back toward the spacecraft.

For every three-spacecraft event, we assigned a class to each spacecraft based on the 10 MeV n^{-1} He time profiles and the

Table 4
Presence of ICMEs, Reservoirs, and ESPs

Event	ICME Class			Reservoir Present[a]			ESP Present[b]		
	STB	*ACE*	*STA*	*STB*	*ACE*	*STA*	*STB*	*ACE*	*STA*
2011/265	4	3	0	…	…	…	…	…	…
2011/308	0	4	0	yes	…	yes	0.3, 1	…	0.3, 1
2012/023	0	4, 3	0	…	yes	yes	…	…	…
2012/027	0	0	4	…	…	…	…	…	all
2012/067	0	4	4	…	…	…	…	0.3, 1	…
2013/231	0	1?	0	yes?	…	yes?	…	…	0.3, 1
2013/347	0	0	0	…	…	…	…	…	
2013/360	0	4	4	yes	yes	…	0.3, 1	…	0.3, 1
2014/008	0	0	0	…	…	…	…	…	all
2014/056	4	4	4	…	…	…	…	…	0.3, 1

Notes.
[a] "yes?" indicates that the reservoir signature is not very clear but might be present.
[b] He energy (0.3, 1, 10 MeV/n) at which an ESP event is evident.

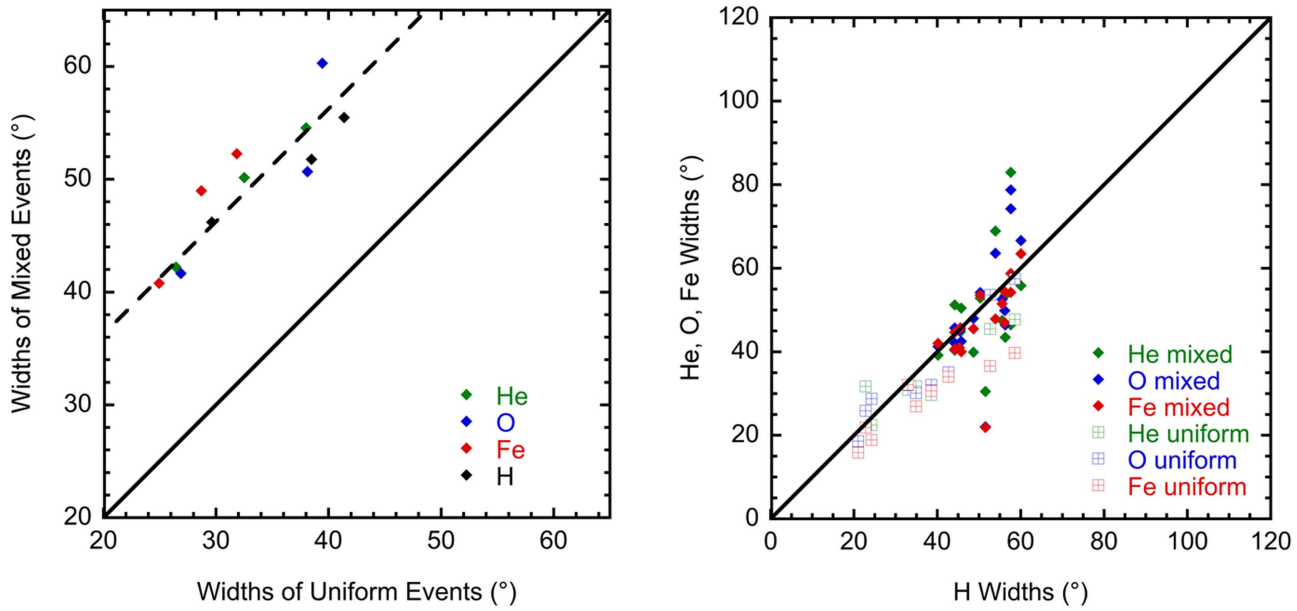

Figure 16. Comparison of widths from events of mixed ICME class vs. uniform ICME class for the average widths (left) and individual event widths (right). All three energies and four species are included.

list of identified ICMEs. Most events had at least one spacecraft in classes 3 or 4; no event had a spacecraft in classes 1 or 2 (except for possibly 2013/231 where the 10 MeV n^{-1} He was unavailable and 10 MeV n^{-1} O was examined instead). We divided the events into two groups: "uniform": events with all three spacecraft in the same class (3 events); and "mixed": events with one or two spacecraft in classes 1, 3 or 4 (6 events) and the other spacecraft in class 0 (event 2013/231 was not put into a group). We have averaged the widths (for each energy and element) of the events in each class and compared them in the left panel of Figure 16, while the right panel compares the He, O, and Fe widths to those of H for each individual event, identified as either a mixed or uniform event.

It is evident in both representations that the mixed events are typically wider than the uniform events. The average widths of the mixed events are wider by ~17°, relatively independent of species or energy. Similarly, the individual event widths reveal that most of the mixed events have widths larger than most of the uniform events, again fairly independent of species, though there is some overlap between the two distributions. This is generally consistent with the observations of Lario and Karelitz since, with the exception of event 2012/023, in the mixed events the spacecraft in class 3 or 4 is not the spacecraft closest to the center of the distribution. An increased fluence at a spacecraft farther from the center of the distribution will result in a larger calculated width than if no (or all) spacecraft had increased fluences due to the presence of an ICME (i.e., a uniform event) or only the central spacecraft had an increased fluence.

4.2. Particle Reservoirs

We searched for evidence of particle reservoirs by comparing the proton intensity-time profiles of the three observing spacecraft at 1 and 5 MeV. Events for which the intensities measured at each spacecraft roughly equaled and tracked each other during the decay phase were identified as particle reservoir periods. Only three events exhibited reservoir behavior between two spacecraft (Table 4). Of these, in two

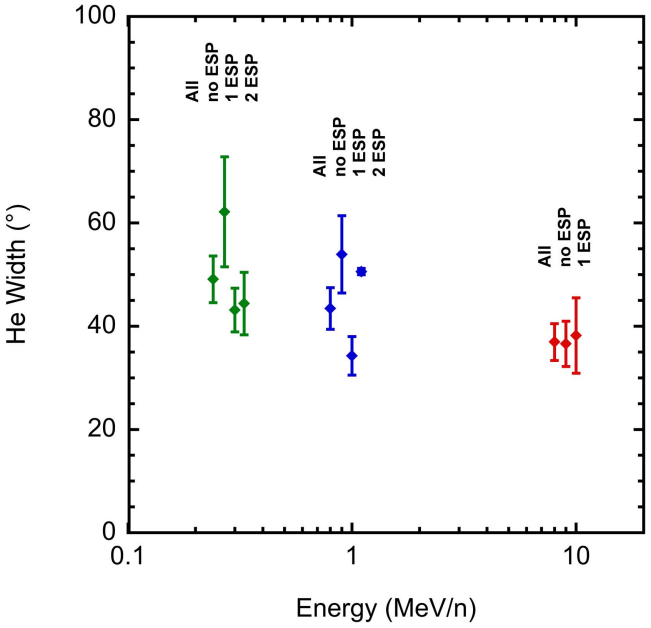

Figure 17. Comparison of average He widths for three-spacecraft events showing different ESP signatures. Note that the same events may fall into different categories at different energies. The points are shifted in energy for each grouping for clarity.

of the events, the reservoir period occurred during the last day of the selected event period when the intensities were an order of magnitude reduced from the peak of the event. Given that the fluences are dominated by the peak intensities, it is expected that the effect of any reservoir in these cases is negligible. The remaining event, 2012/023, has calculated H widths of 60°, 56°, and 46° at 0.3, 1, and 10 MeV, larger than the average H widths of 49°, 46°, and 39°. Thus it is possible that the presence of a reservoir period during the decay of this event created a wider distribution; however, removing this event and recalculating the three-spacecraft average values yields values well within the uncertainties of those determined previously. Thus, while particle reservoirs were present in some three-spacecraft events, they did not significantly influence our deduced average centers or widths.

4.3. Energetic Storm Particle Events

We examined the He intensity-time profiles at each spacecraft at 0.3, 1, and 10 MeV n^{-1} for evidence of ESP events, which might increase the measured fluence. We used a shock list provided by the Heliospheric Shock Database (ipshocks.fi) and noted those three-spacecraft events where the He intensities significantly increased at a shock passage (Table 4). In Figure 17 , we compare the average He width at each energy for the three-spacecraft events divided into three distinct groups: those with no ESP signature at any spacecraft, those with an ESP signature at one spacecraft and those with ESP signatures at two spacecraft (there were no events with ESP events at all three spacecraft). The event groupings were the same for 0.3 and 1 MeV n^{-1}, but at 10 MeV n^{-1} only two events had ESP signatures at one spacecraft and the rest had no ESP signatures at any spacecraft. At the lower energies, the events with no ESP signature are wider than the one-spacecraft ESP events, but this is not the case at 10 MeV n^{-1}. This behavior can be understood if the ESP spacecraft is closest to the center of the distribution; however, of the five one-spacecraft ESP events, only two were consistent with this scenario. It might be possible to subtract the contribution of the ESP to the event-averaged fluence to determine the effect on the calculated Gaussian width for each event, but that is beyond the scope of this work.

4.4. Magnetic Connection at 30 R_S

Although it has been standard in SEP longitude studies to consider the magnetic footpoint of the spacecraft at the photosphere (see, e.g., Lario et al. 2006, 2013; Cohen et al. 2014a), if the particle acceleration is occuring at significant heights in the corona above the flaring region, using the photospheric footpoint may provide misleading results. To investigate this further, we have redone the longitude fits for the three-spacecraft events using the longitude of the spacecraft magnetic field line at 30 R_S (as reported by the Predictive Science online tools). In most events, this does not substantially change the longitude distribution (e.g., event 2011/265 shown in the left panel of Figure 18), but in a few cases the change is significant (e.g., event 2014/056 shown in the right panel of Figure 18). A comparison of all the derived widths using the photospheric footpoints and using the 30 R_S footpoints is given in Figure 19; the periodic Gaussian parameters using the 30 R_S footpoints are given in Table 5 in the same manner as Table 3. As can be seen, for most of the events (energies and elements), the two calculations yield centers that are within ±30° and widths within ±10° of each other, indicating that we have not introduced a systematic bias into the data through the footpoint calculations. The main width exceptions are from events 2014/008 and 2014/056. This is likely because the two *STEREO* spacecraft are quite close together during these events, yet observe very different fluences; thus a larger change in footpoint position (at 30 R_S compared to at the photosphere) for one of the two *STEREOs* can have a dramatic impact on the calculated width (e.g., right panel of Figure 18).

The longitude distribution of 2014/056 has been examined in energetic electrons by Klassen et al. (2016). They noted that although *STB* was nominally better connected to the flaring region, *STA* observed higher peak intensities of 55–65 keV electrons, making it impossible to fit the peak intensities to a Gaussian centered at the flare location. This was not the case for the 0.7–3 MeV electrons, where they obtained a Gaussian width of 47°, substantially wider than the 16°–32° values we obtained for this event (however, our fit was not constrained to be centered at 0°; in fact, the calculated centers were significantly offset from 0°). Using the footpoints at 30 R_S does yield higher width values (21°–50°) in this event. In either case, it appears that the ions generally exhibit narrower distributions than the electrons in this event, opposite to what might be expected from rigidity-dependent cross-field diffusion.

5. Conclusions

We have examined the longitudinal dependence of SEPs in 41 large events observed by the *STEREO*, *ACE*, *SOHO*, and *GOES* spacecraft. Periodic Gaussian distributions were fit to the aggregate two-spacecraft data for H, He, O, and Fe at 0.3, 1, and 10 MeV n^{-1}. Ten events were observed by both *STEREOs* and *ACE*, allowing longitude distributions to be determined individually for each event. For 12 additional events H fluences

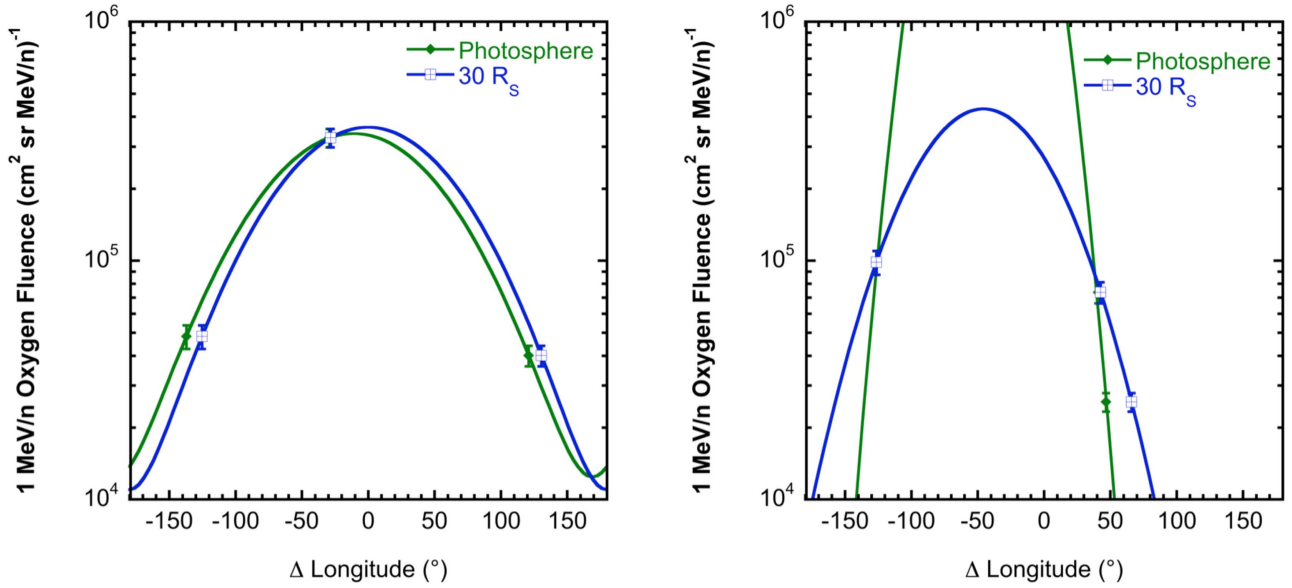

Figure 18. Distributions of 1 MeV n^{-1} O using footpoints calculated at the photosphere (green curves and points) and at 30 R_S (blue curves and points). (Left) The 2011/265 event shows a slight shift in the center of the distribution but not a significant change in width, and (right) the 2014/056 shows a dramatic change in width due to the *STA* footpoint moving from 47° (at the photosphere) to 66° (at 30 R_S), a much larger shift than the other spacecraft footpoints.

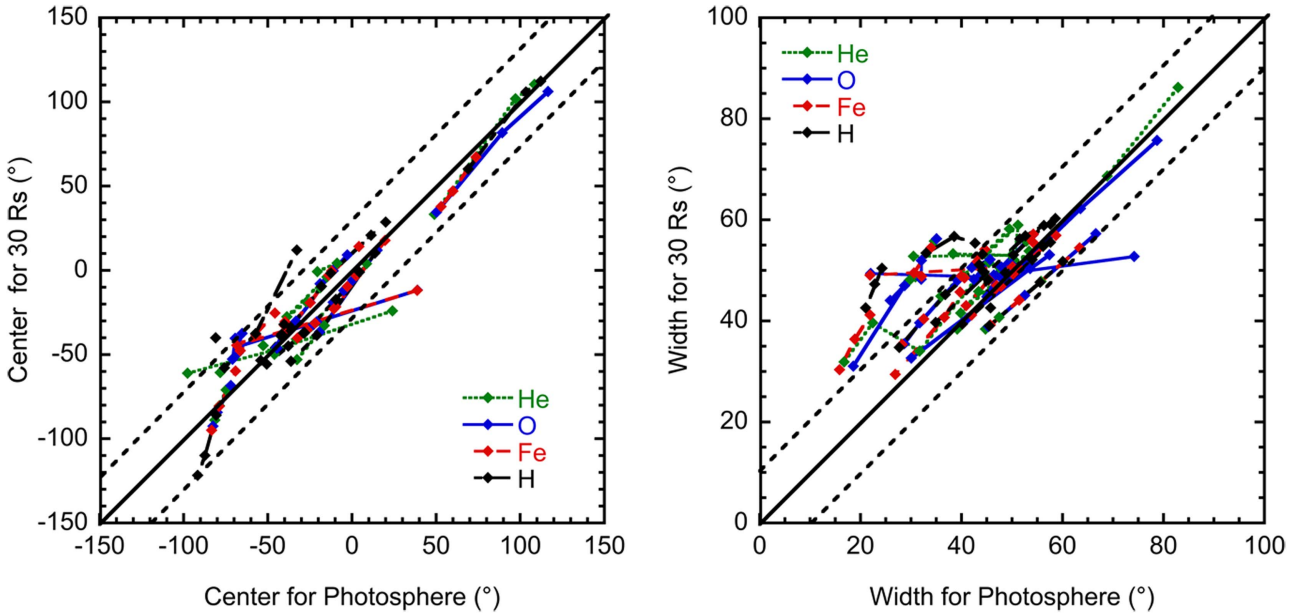

Figure 19. Comparison of calculated centers and widths using the spacecraft footpoint at the photosphere vs. using the footpoint at 30 R_S. Lines connect the different energy calculations for a given event. The heavy diagonal line indicates perfect agreement, the dashed lines on either side mark ±30° (left) and ±10° (right).

were available at all three-spacecraft even though heavy ion fluences were measured at only two; for these events, we used the derived Gaussian center of the proton distribution as the assumed center of the heavy ion distributions and calculated the widths accordingly. By examining several ion species at three distinct energies, we have systematically investigated the energy and Q/M dependence of the longitudinal distributions for the first time.

On average, we find distributions that are centered at $-22 \pm 4°$ and have widths of $43 \pm 1°$ for the three-spacecraft events. This is similar to that found in previous studies. The aggregate fits to the two-spacecraft events yield significantly wider distributions at 0.3 and 1 MeV n^{-1}, which is likely due to significant event-to-event variability (both in the centers and widths of the distributions), which cannot easily be removed. Both the two- and three-spacecraft widths show an energy dependence with the distributions narrowing with increasing energy. This is consistent with the lower energy ions being accelerated and released over a larger portion of the shock or for a longer time period over which the shock expands. It could also result from more field line co-rotation experienced by the slower ions. Surprisingly, there is no clear dependence of either the centers or widths on elemental charge-to-mass ratio. This suggests that cross-field diffusion and other ridigity-related processes are not the dominant means of particle spread in longitude.

Table 5
Periodic Gaussian Centers and Widths for Three-spacecraft Events Using 30 R_S Footpoints

Event	Elmnt	Centers (°)			Widths (°)		
		0.3 MeV n^{-1}	1 MeV n^{-1}	10 MeV n^{-1}	0.3 MeV n^{-1}	1 MeV n^{-1}	10 MeV n^{-1}
2011/265	H	29	21	−1.7	56	52	39
	He	−19	−28	−4.0	86	69	38
	O	9.1	−0.24	−8.0	76	62	40
	Fe	14	−1.9	−2.8	57	47	41
2011/308	H	−54	−39	10	43	50	53
	He	−53	−33	4.0	52	59	49
	O	−38	−37	12	48	52	51
	Fe	−23	−22	18	49	54	49
2012/023	H	−56	−45	−37	52	48	39
	He	−41	−34	−32	48	41	38
	O	−32	−31	−32	57	45	39
	Fe	−40	−31	−35	54	44	39
2012/027	H	−54	−34	−9.4	55	50	48
	He	−0.77	4.2	−10	54	42	48
	O	−30	−19	0.072	51	51	45
	Fe	−38	−19	−0.39	47	48	43
2012/067	H	12	−38	−58	59	59	53
	He	−49	−61	−52	49	46	56
	O	−40	−53	−49	53	49	57
	Fe	−25	−48	−48	56	57	56
2013/231	H	−37	−17	−1.1	51	45	35
	He	−33	−5.1	…	58	45	…
	O	−19	−5.8	−12	48	40	35
	Fe	−9.6	−3.3	…	40	35	…
2013/347	H	110	110	60	60	57	40
	He	110	102	33	50	52	34
	O	110	82	34	53	50	33
	Fe	67	47	38	46	41	29
2013/360	H	−78	−70	−40	51	45	56
	He	−61	−47	−24	53	53	53
	O	−37	−45	−12	49	49	49
	Fe	−38	−45	−12	49	51	49
2014/008	H	−120	−110	−86	55	57	53
	He	−89	−80	−71	56	48	49
	O	−92	−84	−68	56	52	48
	Fe	−95	−81	−60	54	49	49
2014/056	H	−38	−39	−32	47	50	43
	He	−45	−50	−31	34	40	32
	O	−46	−46	−32	44	47	31
	Fe	−33	−32	−30	41	36	30

We have examined the influence of unrelated ICMEs, reservoirs, ESP events, and the calculation of spacecraft magnetic footpoint on the derived distribution widths. We find that the presence of ICMEs can widen the observed distribution by increasing the intensities observed by one or two spacecraft but not affecting all spacecraft. We did not find a significant impact on our results due to the presence of either reservoirs or ESP events. For most events, the derived centers and widths using footpoints at 30 R_S versus the photosphere differed by less than 30° and 10°, respectively. However, in a couple of events for which the two *STEREO* spacecraft were close together, the difference between the spacecraft footpoint longitude at 30 R_S and that at the photosphere was signficantly different for the two spacecraft, which combined with unequal fluences measured by the two spacecraft, led to substantial changes in the derived widths.

The authors thank the *STEREO*/SEPT, *STEREO*/SECCHI, *STEREO*/WAVES, *SOHO*/EPHIN, *Wind*/WAVES, and *SDO*/AIA teams for making their data publicly available, Predicitve Science Inc. for their publicly available model-based field line tracing, L. Jian for her *STEREO* ICME list, and I. Richardson and H. Cane for their near-Earth ICME list. This work was supported by NSF grants 1156004 and 1156138 and NASA grants NNX11075G, NNX13AH66G, and NNX15AG09G. Work at Johns Hopkins University APL was supported by NASA grant NNX17AC05G/125225, and University of California Berkeley grant 00008934. This paper uses data from the CACTus CME catalog, generated and maintained by the SIDC at the Royal Observatory of Belgium; the Heliospheric Shock Database, generated and maintained at the University of Helsinki; and the *SOHO* CME catalog, generated and maintained at the CDAW Data Center by NASA and the Catholic University of America in cooperation with the Naval Research Laboratory (*SOHO* is a project of international cooperation between ESA and NASA). The *GOES* 8-15 particle data are produced in real time by the NOAA Space Weather Prediction Center (SWPC) and are distributed by the NOAA National Geophysical Data Center (NGDC).

References

Band, D., Matteson, J., Ford, L., et al. 1993, ApJ, 413, 281
Cane, H. V. 1988, JGR, 93, 1
Cane, H. V., McGuire, R. E., & von Rosenvinge, T. T. 1986, ApJ, 301, 448
Cane, H. V., Mewaldt, R. A., Cohen, C. M. S., & von Rosenvinge, T. T. 2006, JGR, 111, A06S90
Cane, H. V., Reames, D. V., & von Rosenvinge, T. T. 1988, JGR, 93, 9555
Cane, H. V., von Rosenvinge, T. T., Cohen, C. M. S., & Mewaldt, R. A. 2003, GeoRL, 30, 8017
Cliver, E. W., Kahler, S. W., Neidig, D. F., et al. 1995, Proc. ICRC (Rome), 24, 257
Cliver, E. W., Thompson, B. J., Lawrence, G. R., et al. 2005, Proc. ICRC (Pune), 29, 121
Cohen, C. M. S., Cummings, A. C., Leske, R. A., et al. 1999, GeoRL, 26, 149
Cohen, C. M. S., Mason, G. M., Mewaldt, R. A., et al. 2008, in AIP Conf. Proc. 1039, Particle Acceleration And Transport In The Heliosphere And Beyond, ed. G. Li, et al. (Melville, NY: AIP), 118
Cohen, C. M. S., Mason, G. M., Mewaldt, R. A., & von Rosenvinge, T. T. 2013, in AIP Conf. Proc., 1539, SOLAR WIND 13: Proc. Thirteenth Int. Solar Wind Conf., ed. G. P. Zank, et al. (Melville, NY: AIP), 151
Cohen, C. M. S., Mason, G. M., Mewaldt, R. A., & Wiedenbeck, M. E. 2014a, ApJ, 793, 35
Cohen, C. M. S., Mewaldt, R. A., & Mason, G. M. 2014b, in ASP Conf. Ser., 484, Outstanding Problems in Heliophysics: From Coronal Heating to the Edge of the Heliosphere, ed. Q. Hu & G. P. Zank (San Francisco, CA: ASP), 24
Dalla, S., Marsh, M. S., & Battarbee, M. 2017, ApJ, 834, 167
de Lucas, A., Schwenn, R., dal Lago, A., Marsch, E., & Clúa de Gonzalez, A. L. 2011, JASTP, 73, 1281
Desai, M. I., Mason, G. M., Dayeh, M. A., et al. 2016, ApJ, 816, 68
Dresing, N., Gómez-Herrero, R., Heber, B., et al. 2014, A&A, 567, A27
Giacalone, J., & Jokipii, J. R. 2001, AdSpR, 27, 461
Giacalone, J., & Jokipii, J. R. 2012, ApJL, 751, L33
Gold, R. E., Krimigis, S. M., Hawkins, S. E., et al. 1998, SSRv, 86, 541
Kahler, S. W. 2016, ApJ, 819, 105
Klassen, A., Dresing, N., Gómez-Herrero, R., Heber, B., & Müller-Mellin, R. 2016, A&A, 593, A31
Lario, D., Aran, A., Gómez-Herrero, R., et al. 2013, ApJ, 767, 41
Lario, D., Kallenrode, M.-B., Decker, R. B., et al. 2006, ApJ, 653, 1531
Lario, D., & Karelitz, A. 2014, JGRA, 119, 4185
Lario, D., Roelof, E. C., & Decker, R. B. 2014, in ASP Conf. Ser., 484, Outstanding Problems in Heliophysics: From Coronal Heating to the Edge of the Heliosphere, ed. Q. Hu & G. P. Zank (San Francisco, CA: ASP), 98
Lee, M. A. 2005, ApJ, 158, 38
Li, G., Zank, G. P., & Rice, W. K. M. 2005, JGRA, 110, A06104
Linker, J. A., Mikić, Z., Biesecker, D. A., et al. 1999, JGR, 104, 9809
Luhmann, J. G., Curtis, D. W., Schroeder, P., et al. 2008, SSRv, 136, 117
Luhn, A., Hovestadt, D., Klecker, B., et al. 1985, Proc. ICRC (La Jolla), 19, 24
Mason, G. M., Cohen, C. M. S., Cummings, A. C., et al. 1999, GeoRL, 26, 141
Mason, G. M., Gloeckler, G., & Hovestadt, D. 1984, ApJ, 280, 902
Mason, G. M., Gold, R. E., Krimigis, S. M., et al. 1998, SSRv, 86, 409
Mason, G. M., Korth, A., Walpole, P. H., et al. 2008, SSRv, 136, 257
Mewaldt, R., Cohen, C., Haggerty, D., et al. 2003, Proc. ICRC (Trukuba), 28, 3313
Mewaldt, R. A., Cohen, C. M. S., Cook, W. R., et al. 2008, SSRv, 136, 285
Mewaldt, R. A., Cohen, C. M. S., Mason, G. M., et al. 2013, in AIP Conf. Ser., 1539, SOLAR WIND 13: Proceedings of the Thirteenth International Solar Wind Conference, ed. G. P. Zank, et al. (Melville, NY: AIP), 116
Mewaldt, R. A., Looper, M. D., Cohen, C. M. S., et al. 2012, SSRv, 171, 97
Müller-Mellin, R., Böttcher, S., Falenski, J., et al. 2008, SSRv, 136, 363
Müller-Mellin, R., Kunow, H., Fleißner, V., et al. 1995, SoPh, 162, 483
Ng, C. K., Reames, D. V., & Tylka, A. J. 2003, ApJ, 591, 461
Nolte, J. T., & Roelof, E. C. 1973, SoPh, 33, 483
Reames, D. V. 1998, SSRv, 85, 327
Reames, D. V. 1999, SSRv, 90, 413
Reames, D. V., Ng, C. K., & Tylka, A. J. 2013, SoPh, 285, 233
Richardson, I. G., von Rosenvinge, T. T., Cane, H. V., et al. 2014, SoPh, 289, 3059
Shea, M. A., & Smart, D. F. 1990, SoPh, 127, 297
Stone, E. C., Cohen, C. M. S., Cook, W. R., et al. 1998a, SSRv, 86, 357
Stone, E. C., Frandsen, A. M., Mewaldt, R. A., et al. 1998b, SSRv, 86, 1
Tylka, A. J., Cohen, C. M. S., Dietrich, W. F., et al. 2005, ApJ, 625, 474
Van Hollebeke, M. A. I., Ma Sung, L. S., & McDonald, F. B. 1975, SoPh, 41, 189
Wiedenbeck, M., Mason, G. M., Cohen, C. M. S., et al. 2011, Proc. ICRC (Beijing), 32, 208
Wiedenbeck, M. E., Mason, G. M., Cohen, C. M. S., et al. 2013, ApJ, 762, 54
Zank, G. P., Li, G., & Verkhoglyadova, O. 2007, SSRv, 130, 255
Zhang, M., Jokipii, J. R., & McKibben, R. B. 2003, ApJ, 595, 493